Journal of Sound and Vibration 483 (2020) 115425

Contents lists available at ScienceDirect

Journal of Sound and Vibration

journal homepage: www.elsevier.com/locate/jsvi

A framework for the propagation of uncertainty in Transfer Path Analysis

J.W.R. Meggitt [a,*], A.T. Moorhouse [a], K. Wienen [b], M. Sturm [b]

[a] Acoustics Research Centre, University of Salford, Greater Manchester, UK
[b] Robert Bosch Automotive Steering LLC, Plymouth, MI, USA

ARTICLE INFO

Article history:
Received 28 November 2019
Revised 28 April 2020
Accepted 29 April 2020
Available online 7 May 2020
Handling Editor: D.J. Thompson

Keywords:
Transfer Path Analysis
In-situ
Component
Blocked force
Dynamic sub-structuring
Uncertainty propagation

ABSTRACT

Transfer Path Analysis (TPA) is a test-based methodology used to analyse the propagation of noise and vibration in complex systems. In this paper we present a covariance based framework for the propagation of experimental uncertainty in classical, blocked force, and component-based TPA procedures. The presence of both complex and correlated uncertainty is acknowledged through a bivariate description of the underlying uncertainty. The framework is summarised by a series of equations that propagate uncertainty through the various stages of a TPA procedure i.e. inverse source characterisation, dynamic sub-structuring, and forward response prediction. The uncertainty associated with rank ordering of source contributions is also addressed. To demonstrate the proposed framework a numerical simulation is presented, the results of which are compared against Monte-Carlo methods with good agreement obtained. An experimental study is also presented, where a blocked force TPA is performed on an electric steering system. The proposed uncertainty framework requires no additional experimental effort over and above what is performed in a standard TPA and may therefore be readily implemented into current TPA practices.

1. Introduction

Transfer path analysis (TPA) is a diagnostic method used for analysing the propagation of noise and vibration in complex built-up structures, for example, ships, vehicles, trains, etc. It has become an essential tool in the development and refinement of structures whose vibro-acoustic response is of interest. Although an established tool in many industries, it appears as yet few works have considered the uncertainties associated with its application. The principle aim of TPA is to provide an engineer with the information necessary to make informed design changes that benefit both the manufacture and end user. In this sense, it would appear essential that such information is accompanied by a measure of its uncertainty. With this in mind, it is the aim of the present paper to establish an appropriate framework for the propagation of uncertainty in the context of TPA.

Over the years a variety of TPA methodologies have been proposed (the reader is referred to Ref. [1] for a detailed review of their history and development). Common to all methods is the division of an assembly into active and passive components. Active components are regarded as those that contain vibration generating mechanisms (such as engines, gearboxes, pumps, motors, etc.), whilst passive components simply transmit, and/or radiate, this vibration (for example, vibration isolators, body panels, etc.). It is the role of TPA to predict the contribution of each active component to the total vibro-acoustic response

* Corresponding author.
E-mail address: j.w.r.meggitt1@salford.ac.uk (J.W.R. Meggitt).

https://doi.org/10.1016/j.jsv.2020.115425

at some specified position, e.g. the noise level experienced by a vehicle occupant. To do so the activity, or 'strength', of each active component must first be estimated. Then, the transmission paths through which these components contribute must be identified. Depending on the type of TPA considered, the methods employed and quantities obtained will differ. In this paper we are concerned with blocked force based procedures, namely the blocked force and component-based variants of TPA. Note however, that the proposed uncertainty framework will be equally applicable to classical (matrix inverse) TPA, as the underlying equations are of an identical form (they require solving an inverse problem by matrix inversion).

Force-based TPA relies on a two part measurement procedure.[1] In part one the passive properties (i.e frequency response functions) of the structure of interest are measured between the source-receiver (active-passive) interface[2] and some set of indicator positions, which may or may not include interface degrees of freedom (DoFs). In part two the structure is operated and its activity (i.e. operational acceleration, velocity, etc.) is recorded at the indicator positions (as used in the passive stage). Based on the measured frequency response functions (FRFs), the operational responses are used to infer the unknown excitation force at the defined source-receiver interface. Inverse problems of this nature are notoriously sensitivity to experimental error, making a rigorous treatment of their uncertainty all the more necessary.

In classical TPA active components are characterised by the contact force that they impart on a receiver structure. This contact force is obtained using FRFs that are measured on the uncoupled receiver structure. Although well established and widely employed, classical TPA is time consuming and often impractical, as it requires the assembly to be dismantled for the FRF measurements. Furthermore, the contact forces obtained are dependent upon the dynamics of the receiver structure, meaning that the effect of a structural modification cannot be investigated.

An alternative procedure, known widely as blocked force TPA (also in-situ TPA), relies on the independent characterisation of active components by their blocked force [2]. These blocked forces are obtained using an in-situ approach developed in Ref. [2], which avoids the need to dismantle the assembly. Originally termed 'In-situ source path contribution analysis' by Elliott et al. [3], blocked force TPA offers 2 distinct advantages over classical TPA:

1) The active components are characterised independently. This means that the same set of blocked forces can be used to excite a range of different assemblies, or be applied in the presence of a structural modification (i.e. they are transferable). This is in contrast to classical TPA, where the contact forces obtained are valid only for the assembly in which they are characterised.
2) The characterisation procedure is performed entirely in-situ. This means that the active components need not be removed from their intended installation, unlike classical TPA which requires the assembly to be dismantled.

The in-situ blocked force approach has seen considerable interest due to its straight forward implementation and transferable source properties, evidenced by its recent standardisation (ISO 20270:2019) [4] and integration into commercially available software packages.

More recently, an alternative yet related approach, known as component-based TPA, has been proposed. Unlike classical or blocked force TPA, which are typically used for diagnostic purposes, component-based TPA serves as a predictive tool, capable of predicting the noise and vibration in complex structures that do not necessarily exist, physically. This is achieved by combining blocked force TPA (more specifically, the in-situ blocked force characterisation) with dynamic sub-structuring (DS) procedures [5] (this merger has previously been known as Virtual Acoustic Prototyping [6,7] and was first demonstrated in Ref. [8]). Component-based TPA allows for the virtual interchange of components in a physically consistent manner, thus providing design engineers with a means to investigate the effect of a structural modification/redesign in the presence of a realistic operational excitation (in the form of a measured blocked force). The introduction of DS further facilitates the coupling of experimental and numerically modelled components to form so called 'hybrid assemblies' [9].

Whilst these TPA procedures can provide invaluable diagnostic information and impressive predictive capabilities, they are known to be sensitive to measurement and other errors. It is perhaps surprising then that comparatively little attention has been devoted to the treatment of uncertainty in TPA. Hence, the aim of this paper is to provide a framework for the propagation of uncertainty in force based (i.e. classical, in-situ, and component-based) TPA. The framework is formulated by acknowledging the uncertainty associated with each stage of a TPA procedure, i.e. the active and passive measurements phase, and also the inverse (source characterisation) and forward (response prediction) calculations involved. Key elements of the proposed framework are the propagation of uncertainty through an inverse (blocked) force characterisation, and also through a dynamic sub-structuring (DS) prediction. The propagation of uncertainty in a blocked force characterisation was recently considered by Meggitt et al. [10] where a covariance based framework was presented. In the present paper we provide an alternative derivation of this approach, leading to a simplified set of expressions which are more readily implemented into computer code. The propagation of uncertainty in FRF based DS was initially investigated by Voormeeren et al. [11] under the assumption of uncorrelated uncertainty. Following work by Meggitt [12], where it was shown that inter-FRF correlation (i.e. the correlation between elements of an FRF matrix) can have a considerable influence on the propagation of uncertainty, Meggitt and Moorhouse [13] proposed a generalised framework for uncertainty propagation in FRF-based DS, valid in the presence of correlated uncertainty. Drawing

[1] Note that 'force based' TPA refers explicitly to those methods that are solved by performing a matrix inverse. TPA methods where forces are measured directly are not considered here, although elements of the proposed framework may be adapted for such approaches.

[2] This 'source-receiver' interface is somewhat arbitrary. Often passive components, for example vibration isolators, are included in the definition of an active component. In this case the source-receiver interface would be that between the bottom of the isolator and the remaining portion of the assembly.

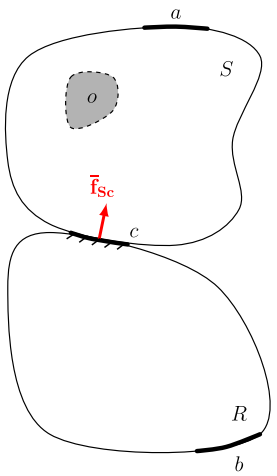

Fig. 1. Diagrammatic representation of a source-receiver (SR) assembly and blocked force.

on these works, in the present paper we formulate a combined framework suitable for propagating (correlated) uncertainty through force-based TPA procedures. In the process we will address the issue of both total response and individual contribution (i.e. rank ordering) uncertainty.

The proposed framework is validated by comparison against Monte-Carlo (MC) simulations. Monte-Carlo methods constitute a broad class of computational algorithms that rely on repeated random sampling to determine a numerical result [14]. In the present context (uncertainty propagation in TPA) the Monte-Carlo method is used to compute blocked forces and response predictions based on the random sampling of measured FRFs and operational responses. Monte-Carlo simulations are advantageous in that they are able to capture the non-linear behaviour of the underlying equations (necessary in the presence of large uncertainty), whilst also providing an estimate of the output's probability distribution. However, covariance-based approaches, such as the framework presented here, bring benefits in terms of reduced computational expense and improved insight.

In TPA, among other related inverse problems, it is common practice to associate confidence in an estimation with the condition number of the measured FRF matrix (or more generally the 'system' matrix) used to determine the acting forces. Whilst it is an established practice to use the condition number as an indicator of the sensitivity of an inverse problem to error, in Ref. [10] it was shown that the condition number was not strongly related to output uncertainty in an experimental setting. This finding will be subject to further scrutiny in the present paper.

The remainder of this paper will be organised as follows. Section 2 will begin by re-introducing the in-situ characterisation of blocked forces. Section 3 will go on to discuss its application, alongside dynamic sub-structuring, in the context of component-based TPA. Section 4 will then focus on formulating the necessary equations for propagating uncertainty through a force-based TPA. The issue of uncertainty in the rank ordering of contributions will be considered in section 5. In section 6 the relation between condition number (often used as an indicator of uncertainty) and the proposed framework will be investigated. Section 7 will discuss the issue of 'systematic' errors related to model completeness and consistency. A numerical validation of the proposed uncertainty framework will then be provided in section 8, before section 9 presents an experimental case study. Finally, section 10 will draw some concluding remarks.

2. Blocked force Transfer Path Analysis

A unique feature of blocked force/component-based TPA is the characterisation of active sub-structures by their blocked force. The blocked force is by definition an invariant source quantity, unaffected by the dynamics of neighbouring sub-structures, i.e it is an independent property of the vibration source. This invariance not only allows for the 'virtual' interchange of sources, but also the modification of receiver structures in a physically consistent manner, a capability not offered by the contact force obtained in a classical TPA.

The blocked force is defined as the reaction force present at the coupling interface of an active sub-structure when its velocity (also displacement and acceleration) is constrained to zero,

$$\bar{\mathbf{f}}_{\mathbf{Sc}} = -\mathbf{f}_{\mathbf{Cc}}|_{\mathbf{v}_{\mathbf{Cc}=\mathbf{0}}} \tag{1}$$

where: lower-case subscript c represents the coupling interface degrees of freedom (DoFs) that separate source and receiver sub-structures (see Fig. 1); upper-case subscripts C and S represent the coupled assembly and the source sub-structure, respectively; and the over-bar accent is used to denote a blocked force, as opposed to a contact force. As a consequence of blocking the interface DoFs c the dynamics of the receiver structure do not influence the blocked force. As such, it provides an independent description of structural source activity.

Classically, a direct measurement of the blocked force required the source in question to be mounted to an approximately rigid test bench, so as to achieve the necessary constraints. This is clearly impractical and achievable only approximately over a particular frequency range. In work by Moorhouse et al. [2] it was shown that the blocked force may instead be acquired through an inverse procedure using measurements performed whilst the source is installed on an arbitrary receiver structure (assuming linearity and time invariance). It has since been acknowledged that this phenomenon is a special case of a general theorem on the representation of fields of forced vibration in composite elastic systems [15]. In the context of structural source characterisation, the relation of note is given by [2],

$$\mathbf{v_{Cb}} = \mathbf{Y_{Cbc}}\bar{\mathbf{f}}_{\mathbf{Sc}} \tag{2}$$

where: $\mathbf{Y_{Cbc}} \in \mathbb{C}^{M\times N}$ is the measured transfer mobility matrix of the coupled assembly, $\mathbf{v_{Cb}} \in \mathbb{C}^{M}$ is a measured operational velocity vector (note that accelerance and acceleration may be used in place of mobility and velocity), and $\bar{\mathbf{f}}_{\mathbf{Sc}} \in \mathbb{C}^{N}$ is the vector of unknown blocked forces. Here, lower-case subscripts b and c represent remote receiver and coupling interface DoFs, respectively (see Fig. 1). Note that the DoF set b may include the interface DoFs c as a subset and that all variables are represented in the frequency domain, with the frequency variable omitted for clarity.

For N = M, providing that the measured mobility matrix is of full rank, a unique solution is found through the inverse mobility matrix $\mathbf{Y}_{\mathbf{Cbc}}^{-\mathbf{1}} = \mathbf{Z_{Ccb}}$, where $\mathbf{Z_{Ccb}} \in \mathbb{C}^{N\times N}$ is an assembly impedance matrix. For M > N, the pseudo-inverse may be used in place of the classical matrix inverse to obtain $\mathbf{Y}_{\mathbf{Cbc}}^{+} = \mathbf{Z_{Ccb}} \in \mathbb{C}^{N\times M}$, leading to a least squares solution of the problem.

Noting that both $\mathrm{Y_{Cbc}}$ and $\mathbf{v_{Cb}}$ are properties of the coupled assembly, Eq. (2) facilitates the in-situ determination of the blocked force. That is, the source need not be installed on a rigid test bench (as would be required for a direct measurement) and may be characterised under 'installed' conditions. The experimental implementation of Eq. (2) follows a two part measurement procedure. In part 1, the source is turned off and the mobility matrix $\mathbf{Y_{Cbc}}$ is measured. Following this, in part 2, the source is operated and the operation velocity $\mathbf{v_{Cb}}$ is measured at the corresponding DoFs. The mobility matrix $\mathbf{Y_{Cbc}}$ relates the DoFs at which the velocity is measured to the coupling interface DoFs where the blocked force is defined. Particular care should be taken during the measurement of $\mathbf{Y_{Cbc}}$ as it must be inverted numerically so as to acquire the blocked force. It is known that poor experimental data is likely to increase the chance of erroneous force estimates, which should be avoided if possible. Often numerical techniques such as regularisation are employed to minimise these effects.

In a blocked force TPA, Eq. (2) is used first to characterise the active components as described above; this can be referred to as the inverse step. Having characterised the blocked force $\bar{\mathbf{f}}_{\mathbf{Sc}}$, Eq. (2) is then used to predict an operational response based on the acquired blocked force; this can be referred to as the forward step, and expressed as,

$$\mathbf{p_{Cr}} = \mathbf{H_{Crc}}\bar{\mathbf{f}}_{\mathbf{Sc}} \tag{3}$$

where: $\mathbf{p_{Cr}} \in \mathbb{C}^{L}$ is the predicted response at some target DoFs r (for example, an interior cabin pressure), and $\mathbf{H_{Crc}} \in \mathbb{C}^{L\times N}$ is a matrix of vibro-acoustic FRFs. The FRF matrix $\mathbf{H_{Crc}}$ is often measured simultaneously to $\mathbf{Y_{Cbc}}$ if excitations are performed at the interface DoFs c. Alternatively, it may be measured reciprocally, for example by using a calibrated volume velocity source. Eqs. (2) and (3) summarize the blocked force TPA procedure.

It should be noted that the forward prediction step, as given by Eq. (3), is used also as an on-board validation procedure, as specified by ISO 20270 [4] (see also [16]). The uncertainty framework proposed herein may prove a helpful tool for users of the ISO standard to understand the origin of potential errors in their on-board validation predictions.

Note that Eq. (2) is identical in form to that of a standard inverse force identification,

$$\mathbf{v_{Cb}} = \mathbf{Y_{Rbc}}\mathbf{f_{Cc}} \tag{4}$$

where: $\mathbf{f_{Cc}}$ represents the contact force present between the source and receiver, and $\mathbf{Y_{Rbc}}$ is the mobility matrix of the uncoupled receiver structure. Eq. (4) is similarly solved through the (pseudo-)inversion of the mobility matrix $\mathbf{Y_{Rbc}}$. In a classical TPA, the contact force, obtained as per Eq. (4), is used to estimate the operational response in a forward prediction step,

$$\mathbf{p_{Cr}} = \mathbf{H_{Rrc}}\mathbf{f_{Cc}} \tag{5}$$

where $\mathbf{H_{Rrc}}$ is the vibro-acoustic FRF matrix of the uncoupled receiver structure. Eqs. (4) and (5) summarize the classical TPA procedure.

In a diagnostic context, Eqs. (3) and (5) are typically broken down as a sum of individual contributions,

$$\mathbf{p_{Cr}} = \sum_i \mathbf{p_{Cr(i)}} = \sum_i \mathbf{H_{Crc_i}}\bar{\mathbf{f}}_{\mathbf{Sc_i}} \tag{6}$$

where $\mathbf{p_{Cr(i)}}$ is the response contribution due to the blocked force $\bar{\mathbf{f}}_{\mathbf{Sc_i}}$, which represents a subset of the acquired blocked forces. The above facilitates a rank ordering of contributions and the identification of potential issues, e.g. a dominant excitation/transmission path.

As noted above, implementation of Eqs. (2) and (3) (also Eqs. (4) and (5)) requires measurement of the operational velocity $\mathbf{v_{Cb}}$, the mobility matrix $\mathbf{Y_{Cbc}}$, and the forward FRF matrix $\mathbf{H_{Crc}}$, all of which are subject to some degree of uncertainty. In the context of a blocked force TPA, we are interested in the influence of this uncertainty on the estimate of the blocked force, $\bar{\mathbf{f}}_{\mathbf{Sc}}$, and the response prediction, $\mathbf{p_{Cr}}$. This propagation of uncertainty will be considered in section 4. Also of interest are the uncertainties of the individual contributions, $\mathbf{p_{Cr(i)}}$. This issue will be discussed further in section 5.

3. Component-based Transfer Path Analysis

In a component-based TPA the forward FRF $\mathbf{H_{Crc}}$ (or $\mathbf{Y_{Crc}}$ if we consider only structural responses) used in Eq. (3) is replaced by a DS prediction for the coupled assembly FRF, thus allowing for the interchange of passive sub-structures. To do so, the dynamics of each constituent sub-structure must be known (whether through experiment or numerical modelling). These are then combined through a primal or dual procedure to obtain the dynamics of the coupled assembly. For completeness we will recall the main DS equations below. For further details the reader is referred to Ref. [5].

The equations of motion for P uncoupled sub-structures may be expressed in a block diagonalised form as,

$$[\mathbf{Z}]\mathbf{v} = \mathbf{f} + \mathbf{g} \tag{7}$$

where, $[\mathbf{Z}]$ is the block diagonal impedance matrix of the P uncoupled sub-structures, $\mathbf{v}$ is the corresponding block vector of velocities, $\mathbf{f}$ is the block vector of applied forces, and $\mathbf{g}$ the block vector of coupling interface forces,

$$[\mathbf{Z}] = \begin{bmatrix} \mathbf{Z^{(1)}} & & & \\ & \mathbf{Z^{(2)}} & & \\ & & \ddots & \\ & & & \mathbf{Z^{(P)}} \end{bmatrix}, \quad \mathbf{v} = \begin{pmatrix} \mathbf{v^{(1)}} \\ \mathbf{v^{(2)}} \\ \vdots \\ \mathbf{v^{(P)}} \end{pmatrix}, \quad \mathbf{f} = \begin{pmatrix} \mathbf{f^{(1)}} \\ \mathbf{f^{(2)}} \\ \vdots \\ \mathbf{f^{(P)}} \end{pmatrix}, \quad \mathbf{g} = \begin{pmatrix} \mathbf{g^{(1)}} \\ \mathbf{g^{(2)}} \\ \vdots \\ \mathbf{g^{(P)}} \end{pmatrix}. \tag{8}$$

The rigid coupling of any two sub-structures is governed by the conditions of compatibility and equilibrium. These may be expressed generally in the form,

$$\mathbf{Bv} = \mathbf{0}, \tag{9}$$

and

$$\mathbf{L^T g} = \mathbf{0}, \tag{10}$$

respectively, where $\mathbf{B}$ and $\mathbf{L}$ represent signed and unsigned Boolean matrices, respectively. Together, equations (7)-(10) are referred to as the three field formulation, and may be solved in a primal or dual manner [5].

3.1. Primal solution

The primal solution involves the definition of a unique set of boundary DoFs that belong to the coupled assembly. The condition of compatibility is consequently expressed in the form,

$$\mathbf{v} = \mathbf{L}\mathbf{v_C}, \tag{11}$$

where $\mathbf{v_C}$ is the velocity of the coupled assembly. Substitution of Eqs. (11) and (10) into Eq. (7) leads to an expression for the mobility of the coupled assembly in the form,

$$\mathbf{Y_C} = \left(\mathbf{L}[\mathbf{Y}]^{-\mathbf{1}}\mathbf{L^T}\right)^{-\mathbf{1}} \tag{12}$$

where $[\mathbf{Y}]$ is the block diagonal (uncoupled) mobility matrix, $\mathbf{Y} = [\mathbf{Z}]^{-\mathbf{1}}$.

3.2. Dual solution

In a dual solution the equilibrium condition is satisfied a priori by choosing the interface force in the form,

$$\mathbf{g} = -\mathbf{B^T}\lambda \tag{13}$$

where λ is a vector of Lagrange multipliers. Noting that the matrix $\mathbf{L}$ lies in the null space of $\mathbf{B}$ (see Ref. [5]), Eq. (10) is always satisfied as it can be written in the form,

$$\mathbf{L^T g} = -\mathbf{L^T B^T}\lambda = \mathbf{0}. \tag{14}$$

Substitution of Eq. (13) into Eq. (7), whilst noting Eq. (9), leads to an expression for the coupled assembly mobility, $\mathbf{Y_C}$, in the form,

$$\mathbf{Y_C} = [\mathbf{Y}] - [\mathbf{Y}]\mathbf{B^T}\left(\mathbf{B}[\mathbf{Y}]\mathbf{B^T}\right)^{-\mathbf{1}}\mathbf{B}[\mathbf{Y}]. \tag{15}$$

Note that the coupled mobility matrix $\mathbf{Y_C}$ obtained through the dual formulation is larger than that obtained via the primal approach, as all uncoupled DoFs are retained. Care must be taken to remove duplicate rows and columns prior to application within a component-based TPA.

In practice, DS procedures require measurement of one or more sub-structure FRF matrices (unless all components are modelled numerically). To provide an accurate estimate of the uncertainty in a component-based TPA response prediction, the uncertainty in the forward FRF matrix $\mathbf{H_{Crc}}$ must be known. If this FRF is predicted through a DS procedure then the uncertainty in

each constituent sub-structure, $\mathbf{Y}^{(\mathbf{P})}$, must first be propagated onto the coupled assembly, $\mathbf{H}_{\mathbf{Crc}}$. The issue of uncertainty propagation through FRF based DS will be recalled from Ref. [13] in section 4.2.3, and used as part of the TPA uncertainty framework presented here.

4. Propagation of uncertainty in Transfer Path Analysis

In this section we will develop a framework for the propagation of uncertainty through a force based TPA. The framework comprises three main elements: i) the inverse characterisation of active components, ii) the forward prediction of an operational response, and iii) the DS of sub-structures to predict forward (coupled) FRFs. Note that this final element is exclusive to component-based TPA. Some elements of the work presented below are reproduced from the recent publications [10,12,13], an overview of which can be found in Ref. [17]. The reader will be referred to these papers for further details when necessary.

4.1. Complex uncertainty and inter-FRF correlation

Before deriving the uncertainty propagation formulae it is necessary to consider the nature of the underlying uncertainty. In Ref. [10] Meggitt et al. categorize the sources of uncertainty in an inverse force identification as originating from the 'model', the 'source', and the 'experiment'. Model uncertainty describes the uncertainty introduced as a result of simplifying assumptions in the governing equations, for example, linearity, the representation of physical connections by a finite number of degrees of freedom, etc. Source uncertainties arise due to inherent variations (assumed random) in the operation of any active sub-structure. Experimental uncertainty was defined as comprising both measurement and operator uncertainty. The former describes the cumulative effect of noise and other external disturbances in the measurement signal path, whilst the latter describes the effect of inconsistent excitation position/orientation when performing impact-based FRF measurements.

Whilst source and experimental uncertainty may be considered random by nature, strictly speaking, model uncertainty introduces a systematic error rather than a random uncertainty. Nevertheless, these errors are an important reason (possibly the main reason) for poor results in TPA. For completeness, the likely origins of model uncertainty, i.e. incompleteness and inconsistency, will be discussed in section 7. Their influence on the propagation of uncertainty, however, is not considered here. The proposed framework is thus derived under the assumption of random errors, and valid only in the presence of source and experimental uncertainty.

To formulate an appropriate framework one must first consider the issue of complex variables. Eqs. (1) through (15) were considered in the frequency domain, rendering all quantities complex (i.e. having both magnitude and phase). A simple approach to handling complex random variables (RVs) is to treat their real and imaginary components separately. Assuming the uncertainty is of an elliptical form (e.g. Gaussian), a complex RV $H \in \mathbb{C}$ may be characterised by its expectation, $\mathbb{E}[H] = \mathbb{E}[\mathrm{Re}(H)] + i\mathbb{E}[\mathrm{Im}(H)]$, and the bivariate variance-covariance matrix,

$$\mathbf{\Sigma}_H = \begin{bmatrix} \sigma_{\mathrm{Re}(H)\mathrm{Re}(H)} & \sigma_{\mathrm{Re}(H)\mathrm{Im}(H)} \\ \sigma_{\mathrm{Im}(H)\mathrm{Re}(H)} & \sigma_{\mathrm{Im}(H)\mathrm{Im}(H)} \end{bmatrix} \tag{16}$$

where: $\sigma_{\mathrm{Re}(H)\mathrm{Re}(H)}$ is the variance of the real part of H, $\sigma_{\mathrm{Im}(H)\mathrm{Im}(H)}$ is the variance of the imaginary part of H, and $\sigma_{\mathrm{Im}(H)\mathrm{Re}(H)} = \sigma_{\mathrm{Re}(H)\mathrm{Im}(H)}$ is the covariance between them. The above may readily be extended to describe the covariance between two complex RVs,

$$\mathbf{\Sigma}_{H_1H_2} = \begin{bmatrix} \sigma_{\mathrm{Re}(H_1)\mathrm{Re}(H_2)} & \sigma_{\mathrm{Re}(H_1)\mathrm{Im}(H_2)} \\ \sigma_{\mathrm{Im}(H_1)\mathrm{Re}(H_2)} & \sigma_{\mathrm{Im}(H_1)\mathrm{Im}(H_2)} \end{bmatrix}. \tag{17}$$

The notion of covariance raises a second important issue; whether or not two RVs are in fact correlated. In experimental structural dynamics it is often assumed that uncertainty is uncorrelated, as this simplifies its subsequent treatment greatly. However, it was shown in Ref. [12] that there can exist a strong correlation between FRFs when obtained using impact based measurements (i.e. when recording multiple responses simultaneously due to a shared excitation). This inter-FRF correlation was shown to influence greatly the propagation of uncertainty through both inverse procedures [12] and DS predictions [13]. For this reason the propagation formulae presented below are derived generally such that any correlations present are accounted for.

4.2. Blocked force and component TPA

A rigorous treatment of the experimental uncertainty associated with the in-situ blocked force approach was first considered by Meggitt et al. [10]. The authors presented a framework for the inverse (blocked force characterisation) and forward (blocked force TPA prediction) propagation of uncertainty that acknowledged both the complex and correlated nature of the uncertainty present [12]. This framework was based on two steps. The first step meant establishing a bivariate covariance matrix for the impedance matrix used to obtain the blocked force. This required the uncertainty in directly measured FRFs to be propagated through a matrix inversion. This was achieved using a derived set of linear inverse propagation relations [10,12]. In a second step, the impedance and velocity uncertainties are propagated onto the blocked force using a linear covariance propagation. In

section 4.2.1 an alternative derivation of this framework is provided, where the propagation of FRF uncertainty through a matrix inversion, and its further propagation onto the blocked force, are combined into a single step. Doing so allows the framework to be reduced to a simplified set of equations that may more readily be implemented into computer code. The issue of forward propagation is considered in section 4.2.2 where simplified equations are also provided.

4.2.1. Inverse force characterisation

To derive the propagation framework we begin by recalling the in-situ blocked force relation in the form,

$$\bar{\mathbf{f}} = \mathbf{Y}^{+}\mathbf{v} \tag{18}$$

where Eq. (2) has been inverted, and its subscripts omitted for clarity. Eq. (18) represents the 'function' through which we will propagate uncertainty. For generality we will consider both the operational response $\mathbf{v}$ and the FRF matrix $\mathbf{Y}$ as uncertain, with their uncertainty characterised by the bivariate covariance matrices, $\mathbf{\Sigma_v}$ and $\mathbf{\Sigma_Y}$, respectively.

In what follows we will consider a linear covariance propagation of uncertainty. In this approach uncertainties are propagated according to the derivatives of the function of interest. Under the assumptions that i) the uncertainties present are small enough to be treated using a linear covariance propagation and ii) that the FRF and operational response measurements are uncorrelated (this is a fair assumption as they will be obtained from different experiments), the inverse propagation of uncertainty takes the form,

$$\mathbf{\Sigma}_{\bar{\mathbf{f}}} = \mathbf{J_Y}\mathbf{\Sigma_Y}\mathbf{J_Y^T} + \mathbf{J_v}\mathbf{\Sigma_v}\mathbf{J_v^T} \tag{19}$$

where: $\mathbf{\Sigma}_{\bar{\mathbf{f}}}$, $\mathbf{\Sigma_Y}$ and $\mathbf{\Sigma_v}$ are the bivariate covariance matrices of the blocked force vector, the FRF matrix, and the operational response vector, respectively, $\mathbf{J_Y}$ is the bivariate Jacobian matrix associated with FRF uncertainty (i.e. the derivatives of $\bar{\mathbf{f}}$ with respect to $\mathbf{Y}$) and $\mathbf{J_v}$ is the bivariate Jacobian matrix associated with operational response uncertainty (i.e. the derivatives of $\bar{\mathbf{f}}$ with respect to $\mathbf{v}$). Construction of the bivariate covariance matrices will be detailed in section 4.4. The Jacobians $\mathbf{J_Y}$ and $\mathbf{J_v}$ will be derived in the following.

Eq. (19) constitutes the central equation for the inverse propagation of uncertainty, its application however requires that we first compute the bivariate Jacobian matrices $\mathbf{J_Y}$ and $\mathbf{J_v}$. To compute these Jacobians we begin by taking the complex differential of the blocked force vector,

$$\mathrm{d}\bar{\mathbf{f}} = \mathrm{d}(\mathbf{Y}^{+}\mathbf{v}) = \mathrm{d}(\mathbf{Y}^{+})\mathbf{v} + \mathbf{Y}^{+}\mathrm{d}(\mathbf{v}). \tag{20}$$

We will consider first the differential response term, $\mathbf{Y}^{+}\mathrm{d}(\mathbf{v})$. Suppose the small change, represented by the differential $\mathrm{d}(\mathbf{v})$, is limited to a single element of the response vector. In this case the differential may be replaced by the scaled unit vector, $\mathbf{p_i}\mathrm{d}v_i$, where $\mathbf{p_i} = \begin{bmatrix} 0\,0\cdots1\cdots0 \end{bmatrix}^T$ is a zero vector bar the ith entry, whose value is one, and $\mathrm{d}v_i$ is a scalar differential term.

$$\mathrm{d}\bar{\mathbf{f}} = \mathbf{Y}^{+}\mathrm{d}\left(\mathbf{v}\right) \rightarrow \mathrm{d}\bar{\mathbf{f}} = \mathbf{Y}^{+}\mathbf{p_i}\mathrm{d}v_i \tag{21}$$

From Eq. (21) the partial derivative of $\bar{\mathbf{f}}$, with respect to the single response variable v_i, is identified as,

$$\frac{\partial\bar{\mathbf{f}}}{\partial v_i} = \mathbf{Y}^{+}\mathbf{p_i}. \tag{22}$$

To construct the Jacobian matrix $\mathbf{J_v}$ we must compute the derivative of $\bar{\mathbf{f}}$ with respect to each response variable. By horizontally aligning the unit vectors $\mathbf{p_i}$, the resultant matrix becomes the identity matrix $\mathbf{P_i} = \mathbf{I}$, and the left hand side becomes a matrix whose columns correspond to derivatives with respect to each element of the response vector.

Noting that Eq. (22) is analytic and satisfies the Cauchy-Riemann equations (see Appendix B of [10]), the bivariate Jacobian $\mathbf{J_v}$ is obtained by applying, element-wise, the complex matrix mapping operator $M(\,)$,

$$\mathbf{J_v} = M\left(\mathbf{Y}^{+}\right), \tag{23}$$

defined as,

$$M(A) = \begin{bmatrix} \mathrm{Re}\,(A) & -\mathrm{Im}\,(A) \\ \mathrm{Im}\,(A) & \mathrm{Re}\,(A) \end{bmatrix}. \tag{24}$$

Given the blocked force vector $\bar{\mathbf{f}} \in \mathbb{C}^N$, and the operational response vector $\mathbf{v} \in \mathbb{C}^M$, the Jacobian is $\mathbf{J_v} \in \mathbb{R}^{2N\times 2M}$.

Let us now consider the differential FRF term, $\mathrm{d}(\mathbf{Y}^{+})\mathbf{v}$. Note that this differential term is more complex than the previous as it contains a matrix pseudo-inverse, which is not only a non-linear function, but non-analytic (i.e. its derivative depends on both $\mathbf{Y}$ and its conjugate $\mathbf{Y}^{*}$). From Refs. [10,18] the complex differential of the pseudo inverse of $\mathbf{Y}$, with respect to one of its elements, say Y_{st}, is given by,

$$\mathrm{d}\mathbf{Y}^{+} = \left[-\mathbf{Y}^{+}\mathbf{P_{st}}\mathbf{Y}^{+}\right]\mathrm{d}Y_{st} + \left[\mathbf{Y}^{+}\mathbf{Y}^{+\mathbf{H}}\mathbf{P_{ts}}(\mathbf{I}-\mathbf{Y}\mathbf{Y}^{+}) + (\mathbf{I}-\mathbf{Y}^{+}\mathbf{Y})\mathbf{P_{ts}}\mathbf{Y}^{+\mathbf{H}}\mathbf{Y}^{+}\right]\mathrm{d}Y_{st}^{*} \tag{25}$$

where: $\mathbf{P_{st}}$ is a zero matrix bar the stth entry, whose value is one, * represents complex conjugation, and $^\mathbf{H}$ the Hermitian operator (conjugate transpose). Note that in the case of a square matrix the second term in Eq. (25) reduces to the zero matrix (i.e. the standard matrix inverse is analytic), and the analysis that follows simplifies considerably.

By substituting Eq. (25) into the first term of Eq. (20), the complex differential of the blocked force, with respect to the differential FRF element $\mathrm{d}Y_{st}$ and its conjugate, may be rewritten in the form,

$$\mathrm{d}\bar{\mathbf{f}} = -\mathbf{Y}^{+}\mathbf{P_{st}}\mathbf{Y}^{+}\mathbf{v}\mathrm{d}Y_{st} + \left(\mathbf{Y}^{+}\mathbf{Y}^{+\mathbf{H}}\mathbf{P_{ts}}(\mathbf{I}-\mathbf{Y}\mathbf{Y}^{+}) + (\mathbf{I}-\mathbf{Y}^{+}\mathbf{Y})\mathbf{P_{ts}}\mathbf{Y}^{+\mathbf{H}}\mathbf{Y}^{+}\right)\mathbf{v}\mathrm{d}Y^{*}_{st}. \tag{26}$$

To construct the full Jacobian matrix $\mathbf{J_Y}$ (i.e. derivatives with respect to each FRF element) we begin by recalling the vectorisation operator, vec( ), which stacks the columns of the argument matrix into a long column vector (in order left to right) such that, given $\mathbf{A} \in \mathbb{C}^{N\times M}$, $\mathrm{vec}(\mathbf{A}) = \mathbf{a} \in \mathbb{C}^{NM\times 1}$. Using lemma 2.11 from Ref. [18],

$$\mathrm{vec}(\mathbf{ABC}) = (\mathbf{C}^{\mathbf{T}} \otimes \mathbf{A})\mathrm{vec}(\mathbf{B}) \tag{27}$$

where $\otimes$ denotes the Kronecker product (see definition 2.6 of [18]), the vectorisation of Eq. (26) (noting that $\mathrm{vec}(\mathrm{d}\bar{\mathbf{f}}) = \mathrm{d}\bar{\mathbf{f}}$) yields two terms, the first

$$\mathrm{vec}(-\mathbf{Y}^{+}\mathbf{P_{st}}\mathbf{Y}^{+}\mathbf{v}) = -\left((\mathbf{Y}^{+}\mathbf{v})^{\mathbf{T}} \otimes \mathbf{Y}^{+}\right)\mathrm{vec}(\mathbf{P_{st}}) \tag{28}$$

and the second,

$$\begin{aligned}
&\mathrm{vec}\left(\left(\mathbf{Y}^{+}\mathbf{Y}^{+\mathbf{H}}\mathbf{P_{ts}}(\mathbf{I}-\mathbf{Y}\mathbf{Y}^{+}) + (\mathbf{I}-\mathbf{Y}^{+}\mathbf{Y})\mathbf{P_{ts}}\mathbf{Y}^{+\mathbf{H}}\mathbf{Y}^{+}\right)\mathbf{v}\right) = \\
&\left(\left((\mathbf{I}-\mathbf{Y}\mathbf{Y}^{+})\mathbf{v}\right)^{\mathbf{T}} \otimes \mathbf{Y}^{+}\mathbf{Y}^{+\mathbf{H}}\right)\mathrm{vec}(\mathbf{P_{ts}}) + \left((\mathbf{Y}^{+\mathbf{H}}\mathbf{Y}^{+}\mathbf{v})^{\mathbf{T}} \otimes (\mathbf{I}-\mathbf{Y}^{+}\mathbf{Y})\right)\mathrm{vec}(\mathbf{P_{ts}}) = \\
&\left[\left(\left((\mathbf{I}-\mathbf{Y}\mathbf{Y}^{+})\mathbf{v}\right)^{\mathbf{T}} \otimes \mathbf{Y}^{+}\mathbf{Y}^{+\mathbf{H}}\right) + \left((\mathbf{Y}^{+\mathbf{H}}\mathbf{Y}^{+}\mathbf{v})^{\mathbf{T}} \otimes (\mathbf{I}-\mathbf{Y}^{+}\mathbf{Y})\right)\right]\mathrm{vec}(\mathbf{P_{ts}}).
\end{aligned} \tag{29}$$

Eqs. (28) and (29) denote vectors that contain the partial derivatives of each element of $\bar{\mathbf{f}}$ with respect to the single FRF element Y_{st}. Note that as one cycles through the st elements of $\mathbf{P_{st}}$, $\mathrm{vec}(\mathbf{P_{st}})$ represents a unit vector whose index increases with each step. Clearly, by arranging each $\mathrm{vec}(\mathbf{P_{st}})$ as the columns of a matrix we arrive at the identity matrix, $\mathbf{I}$. In doing so, Eq. (28) yields a matrix whose columns represent the derivatives of $\bar{\mathbf{f}}$ with respect to each element of $\mathbf{Y}$. Similarly, by arranging each $\mathrm{vec}(\mathbf{P_{ts}})$ as the columns of a matrix we arrive at the so called 'commutation matrix', $\mathbf{K}$ (see pg. 13 of [18]). The commutation matrix is used for transforming the vectorised form of a matrix into the vectorised form of its transpose. The complex differential is then given by,

$$\mathrm{d}\bar{\mathbf{f}} = -(\mathbf{Y}^{+}\mathbf{v})^{\mathbf{T}} \otimes \mathbf{Y}^{+}\mathrm{vec}(\mathrm{d}\mathbf{Y}) + \left[\left(\left((\mathbf{I}-\mathbf{Y}\mathbf{Y}^{+})\mathbf{v}\right)^{\mathbf{T}} \otimes \mathbf{Y}^{+}\mathbf{Y}^{+\mathbf{H}}\right) + \left((\mathbf{Y}^{+\mathbf{H}}\mathbf{Y}^{+}\mathbf{v})^{\mathbf{T}} \otimes (\mathbf{I}-\mathbf{Y}^{+}\mathbf{Y})\right)\right]\mathbf{K}\mathrm{vec}(\mathrm{d}\mathbf{Y}^{*}) \tag{30}$$

where the vectorised differentials $\mathrm{vec}(\mathrm{d}\mathbf{Y})$ and $\mathrm{vec}(\mathrm{d}\mathbf{Y}^{*})$ are introduced accordingly.

To be compatible with the bivariate description of uncertainty adopted here, the above must be re-expressed in terms of the real and imaginary components of $\bar{\mathbf{f}}$ and $\mathbf{Y}$. As Eq. (30) is non-analytic, the complex matrix mapping operator $M(\ )$ is not applicable. A similar issue was encountered in Ref. [10]. Following the same steps as in Ref. [10] it can be shown that,

$$\begin{aligned}
&\frac{\partial \mathrm{Re}(\bar{\mathbf{f}})}{\mathrm{vec}(\partial \mathrm{Re}(\mathbf{Y}))} = \mathrm{Re}\left(\mathbf{A}+\mathbf{B}\right), \quad \frac{\partial \mathrm{Re}(\bar{\mathbf{f}})}{\mathrm{vec}(\partial \mathrm{Im}(\mathbf{Y}))} = \mathrm{Im}\left(-\mathbf{A}+\mathbf{B}\right) \\
&\frac{\partial \mathrm{Im}(\bar{\mathbf{f}})}{\mathrm{vec}(\partial \mathrm{Re}(\mathbf{Y}))} = \mathrm{Im}\left(\mathbf{A}+\mathbf{B}\right), \quad \frac{\partial \mathrm{Im}(\bar{\mathbf{f}})}{\mathrm{vec}(\partial \mathrm{Im}(\mathbf{Y}))} = -\mathrm{Re}\left(-\mathbf{A}+\mathbf{B}\right)
\end{aligned} \tag{31}$$

where,

$$\mathbf{A} = -(\mathbf{Y}^{+}\mathbf{v})^{\mathbf{T}} \otimes \mathbf{Y}^{+} \tag{32}$$

and

$$\mathbf{B} = \left[\left(\left((\mathbf{I}-\mathbf{Y}\mathbf{Y}^{+})\mathbf{v}\right)^{\mathbf{T}} \otimes \mathbf{Y}^{+}\mathbf{Y}^{+\mathbf{H}}\right) + \left((\mathbf{Y}^{+\mathbf{H}}\mathbf{Y}^{+}\mathbf{v})^{\mathbf{T}} \otimes (\mathbf{I}-\mathbf{Y}^{+}\mathbf{Y})\right)\right]\mathbf{K}. \tag{33}$$

The above relations may be summarised using the modified complex matrix mapping operator, $M_H(A,B)$, defined as,

$$M_H(A,B) = \begin{bmatrix} \mathrm{Re}\left(A+B\right) & \mathrm{Im}\left(-A+B\right) \\ \mathrm{Im}\left(A+B\right) & -\mathrm{Re}\left(-A+B\right) \end{bmatrix}. \tag{34}$$

The bivariate Jacobian $\mathbf{J_Y}$ is then given by,

$$\mathbf{J_Y} = M_H\left(-(\mathbf{Y}^{+}\mathbf{v})^{\mathbf{T}} \otimes \mathbf{Y}^{+}, \left[\left(\left((\mathbf{I}-\mathbf{Y}\mathbf{Y}^{+})\mathbf{v}\right)^{\mathbf{T}} \otimes \mathbf{Y}^{+}\mathbf{Y}^{+\mathbf{H}}\right) + \left((\mathbf{Y}^{+\mathbf{H}}\mathbf{Y}^{+}\mathbf{v})^{\mathbf{T}} \otimes (\mathbf{I}-\mathbf{Y}^{+}\mathbf{Y})\right)\right]\mathbf{K}\right) \tag{35}$$

where $M_H(A, B)$ is applied element-wise. Note again that in the case of a square FRF matrix, the second term in Eq. (35) disappears, and the modified mapping operator, $M_H(A, B)$ reduces to $M(A)$ (i.e the standard matrix inverse is analytic),

$$\mathbf{J_Y} = M\left(-(\mathbf{Y^{-1}v})^{\mathbf{T}} \otimes \mathbf{Y^{-1}}\right). \tag{36}$$

Given the blocked force vector $\bar{\mathbf{f}} \in \mathbb{C}^N$, and the FRF matrix $\mathbf{Y} \in \mathbb{C}^{M\times N}$, the Jacobian is $\mathbf{J_Y} \in \mathbb{R}^{2N\times 2MN}$.

Together, Eqs. (19), (23) and (35) provide the necessary formulae to propagate complex and correlated uncertainty, in both the FRF and operational response measurements, through the inverse characterisation procedure, and onto the blocked force, thus providing an estimate the blocked force bivariate covariance matrix $\mathbf{\Sigma_{\bar{f}}}$. Note that Eqs. (19), (23) and (35) are also applicable in the case of a contact force estimation, where $\mathbf{Y} = \mathbf{Y_C}$ is simply replaced by $\mathbf{Y} = \mathbf{Y_R}$.

Often when solving inverse problems, such as force identification, regularisation methods are used to overcome the issue of an ill-posed or ill-conditioned matrix inversion [19]. Although sometimes beneficial, regularisation complicates the propagation of uncertainty. Depending on the regularisation technique used, the response and/or FRF Jacobians ($\mathbf{J_v}$ and $\mathbf{J_Y}$) derived above may no longer be suitable. New Jacobian matrices must be derived, taking into account the regularisation procedure. Unfortunately, further discussion on this topic is outside the scope of this paper. Alternatively, a Monte-Carlo based propagation may be used. This approach is discussed further in section 4.3.

4.2.2. Forward response prediction

Having estimated the blocked force through an inverse procedure, the forward prediction of an operational response can be made. This forward prediction step applies not only to a TPA response prediction, but also the blocked force on-board validation procedure as standardized by ISO 20270 [4]. In either case, the equation of note is recalled as,

$$\mathbf{p} = \mathbf{H}\bar{\mathbf{f}} \tag{37}$$

where: $\mathbf{p}$ is a vector of operational response predictions (e.g. sound pressure level, structural velocity, etc.), and $\mathbf{H}$ is the corresponding matrix of vibro-acoustic FRFs. Note that subscripts are again omitted for clarity. Under similar assumptions as above, the forward propagation of uncertainty takes the form,

$$\mathbf{\Sigma_p} = \mathbf{J_H}\mathbf{\Sigma_H}\mathbf{J_H^T} + \mathbf{J_{\bar{f}}}\mathbf{\Sigma_{\bar{f}}}\mathbf{J_{\bar{f}}^T} \tag{38}$$

where $\mathbf{\Sigma_p}$, $\mathbf{\Sigma_H}$, and $\mathbf{\Sigma_{\bar{f}}}$ are, respectively, the bivariate covariance matrices of the (TPA) response prediction, the forward FRF matrix, and the blocked force (determined as per section 4.2.1), and $\mathbf{J_H}$ and $\mathbf{J_{\bar{f}}}$ are their associated Jacobian matrices.

As Eq. (37) is a straightforward set of linear equations (i.e. contains no matrix inversions), the Jacobians are derived simply as follows,

$$\mathrm{d}\mathbf{p} = \mathrm{d}(\mathbf{H})\bar{\mathbf{f}} + \mathbf{H}\mathrm{d}(\bar{\mathbf{f}}) \rightarrow \mathrm{vec}(\mathrm{d}(\mathbf{H})\bar{\mathbf{f}}) = \left(\bar{\mathbf{f}}^{\mathbf{T}} \otimes \mathbf{I}\right)\mathrm{vec}(\mathrm{d}\mathbf{H}) \rightarrow \mathbf{J_H} = M\left(\bar{\mathbf{f}}^{\mathbf{T}} \otimes \mathbf{I}\right) \tag{39}$$

and

$$\mathrm{d}\mathbf{p} = \mathrm{d}\left(\mathbf{H}\right)\bar{\mathbf{f}} + \mathbf{H}\mathrm{d}\left(\bar{\mathbf{f}}\right) \rightarrow \mathrm{vec}\left(\mathbf{H}\mathrm{d}\left(\bar{\mathbf{f}}\right)\right) = \left(\mathbf{I} \otimes \mathbf{H}\right)\mathrm{vec}\left(\mathrm{d}\bar{\mathbf{f}}\right) \rightarrow \mathbf{J_{\bar{f}}} = M\left(\mathbf{H}\right) \tag{40}$$

where $M(\,)$ is again applied element-wise. Note that if $\mathbf{H}$ is measured the forward propagation of uncertainty is exact, given that Eq. (37) is linear.

If $\mathbf{H}$ is measured simultaneously to $\mathbf{Y}$ (i.e. the FRF matrix used to calculate the blocked force), then there may exist a non-zero covariance $\mathbf{\Sigma_{H,Y}} = \mathbf{\Sigma^T_{Y,H}}$ between them (due to their shared excitation) which is not accounted for by Eq. (38). To include the influence of this correlation an additional term is required,

$$\mathbf{\Sigma_p} = \mathbf{J_H}\mathbf{\Sigma_H}\mathbf{J_H^T} + \mathbf{J_{\bar{f}}}\mathbf{\Sigma_{\bar{f}}}\mathbf{J_{\bar{f}}^T} + \left[\mathbf{J_H}\mathbf{\Sigma_{H,Y}}\mathbf{J_{HY}^T} + \mathbf{J_{HY}}\mathbf{\Sigma_{Y,H}}\mathbf{J_H^T}\right] \tag{41}$$

where the Jacobian $\mathbf{J_{HY}}$ is given by,

$$\mathbf{J_{HY}} = M_H\left(-(\mathbf{Y^+v})^{\mathbf{T}} \otimes \mathbf{HY^+}, \left[\left(((\mathbf{I} - \mathbf{YY^+})\mathbf{v})^{\mathbf{T}} \otimes \mathbf{HY^+Y^{+H}}\right) + \left((\mathbf{Y^{+H}Y^+v})^{\mathbf{T}} \otimes \mathbf{H}(\mathbf{I} - \mathbf{YY^+})\right)\right]\mathbf{K}\right). \tag{42}$$

Eq. (42) represents the derivative of the response vector $\mathbf{p}$ with respect to the FRF matrix $\mathbf{Y}$. It may be obtained straightforwardly by pre-multiplying the differential blocked force $\mathrm{d}(\bar{\mathbf{f}})$ by the vibro-acoustic FRF $\mathbf{H}$, thus obtaining the differential pressure,

$$\mathrm{d}\mathbf{p} = \mathbf{H}\mathrm{d}(\bar{\mathbf{f}}). \tag{43}$$

Substituting the differential blocked force from Eq. (26) then yields,

$$\mathrm{d}\mathbf{p} = -\mathbf{HY^+P_{st}Y^+v}\mathrm{d}Y_{st} + \left(\mathbf{HY^+Y^{+H}P_{ts}}(\mathbf{I} - \mathbf{YY^+}) + \mathbf{H}(\mathbf{I} - \mathbf{Y^+Y})\mathbf{P_{ts}Y^{+H}Y^+}\right)\mathbf{v}\mathrm{d}Y^*_{st} \tag{44}$$

where d$\mathbf{p}$ represents the small change in the response vector $\mathbf{p}$ resulting from a small change in the FRF element Y_{st}. Vectorisation and application of the complex mapping $M_H(A,B)$ yields the Jacobian $\mathbf{J_{HY}}$, as in Eq. (42). Note that this additional term can lead to a large reduction in the estimated uncertainty, as illustrated in section 8, and should not be neglected.

Given the operational response vector $\mathbf{p} \in \mathbb{C}^L$, the blocked force vector $\bar{\mathbf{f}} \in \mathbb{C}^N$, and the forward FRF matrix $\mathbf{H} \in \mathbb{C}^{L\times N}$, the Jacobians are $\mathbf{J_H} \in \mathbb{R}^{2L\times 2LN}$, $\mathbf{J_{\bar{f}}} \in \mathbb{R}^{2L\times 2N}$, and $\mathbf{J_{HY}} \in \mathbb{R}^{2L\times 2NM}$.

In the case that $\mathbf{H}$ is predicted through some dynamic sub-structuring procedure (e.g. in a component-based TPA), $\mathbf{\Sigma_H}$ will not be directly available and must be calculated based on the uncertainty of the assembly's constituent sub-structures. The propagation of uncertainty through dynamic sub-structuring procedures will be covered as part of the following subsection.

4.2.3. Dynamic sub-structuring and sub-structure decoupling

The propagation of uncertainty through a dynamic sub-structuring procedure (in the FRF domain) was originally considered in Ref. [11], based on the dual formulation under the assumption of uncorrelated uncertainty. Following evidence supporting the influence of inter-FRF correlation [12], Meggitt and Moorhouse derived a more general framework taking into account the covariance between measured FRFs [13]. As above, this framework was based on a linear covariance propagation, and takes the form,

$$\mathbf{\Sigma_{Y_C}} = \mathbf{J}\mathbf{\Sigma}_{[\mathbf{Y}]}\mathbf{J}^{\mathbf{T}}. \tag{45}$$

where: $\mathbf{\Sigma_{Y_C}}$ is the bivariate covariance matrix of the coupled FRF matrix $\mathbf{Y_C}$, $\mathbf{\Sigma}_{[\mathbf{Y}]}$ is the bivariate covariance matrix of the uncoupled FRF matrix $\mathbf{Y}$, and $\mathbf{J}$ is a Jacobian matrix associated with the sub-structuring procedure.

The form of $\mathbf{J}$ will depend on whether a primal or dual formulation is considered. Although primal and dual procedures enforce the same coupling, it was noted in Ref. [13] that if non-square FRF matrices are used, the dual formulation of uncertainty propagation should be considered as it requires only a standard matrix inversion of the interface DoFs (as opposed to a pseudo-inversion of the entire FRF matrix as in the primal case).

Derivations of the primal and dual Jacobians are not presented here, for this the reader is referred to Ref. [13]. In the case that a primal sub-structuring procedure is used (see Eq. (12)), the Jacobian takes the form,

$$\mathbf{J} = \mathbf{J_P} = M\left(\left(\mathbf{Y^{-1}L^{T}Y_C}\right)^{\mathbf{T}} \otimes \left(\mathbf{Y_C L Y^{-1}}\right)\right). \tag{46}$$

In the dual case (see Eq. (15)), the Jacobian is given by,

$$\mathbf{J} = \mathbf{J_D} = M\left(\mathbf{I} - \left[\left(\mathbf{B^{T}}\left(\mathbf{BYB^{T}}\right)^{-\mathbf{1}}\mathbf{BY}\right)^{\mathbf{T}} \otimes \mathbf{I}\right] + \left[\left(\mathbf{B^{T}}\left(\mathbf{BYB^{T}}\right)^{-\mathbf{1}}\mathbf{BY}\right)^{\mathbf{T}} \otimes \mathbf{YB^{T}}\left(\mathbf{BYB^{T}}\right)^{-\mathbf{1}}\mathbf{B}\right] - \left[\mathbf{I} \otimes \mathbf{YB^{T}}\left(\mathbf{BYB^{T}}\right)^{-\mathbf{1}}\mathbf{B}\right]\right). \tag{47}$$

Given the coupled FRF matrix $\mathbf{Y_C} \in \mathbb{C}^{L\times N}$ and the uncoupled FRF matrix $\mathbf{Y} \in \mathbb{C}^{P\times Q}$, the primal and dual Jacobians are $\mathbf{J_P} \in \mathbb{R}^{2LN\times 2PQ}$ and $\mathbf{J_D} \in \mathbb{R}^{2PQ\times 2PQ}$ (note that the dual approach retains the full DoF set).

In both cases the operator $M(\ \ )$ is applied element-wise. It was noted in Ref. [13] that the dual case must be used if the uncoupled FRF matrix $\mathbf{Y}$ is non-square, as this renders the primal procedure non-analytic. Once computed, the coupled FRF's bivariate covariance matrix $\mathbf{\Sigma_{Y_C}}$ may be used in place of $\mathbf{\Sigma_H}$ in Eq. (38) if a component-based TPA is considered. It is noted that the above expressions are valid also in the case of sub-structure decoupling, provided that the necessary changes are made to the Jacobian matrices (e.g. negation of the residual FRF matrix, etc.) [13].

4.3. A combined framework for TPA uncertainty

Having established expressions for propagating uncertainty through the inverse characterisation, forward prediction, and dynamic sub-structuring steps of a TPA, we are now able to formulate the combined framework. Substituting Eqs. (19) and (45) into Eq. (38) yields an expression for the bivariate uncertainty in a component-based TPA prediction in terms of the uncertainty in each experimental step (i.e. measurement of $\mathbf{v}$, $\mathbf{Y}$ and $\mathbf{Y^{(P)}}$),

$$\mathbf{\Sigma_p} = \mathbf{J_H}\left(\mathbf{J}\mathbf{\Sigma}_{[\mathbf{Y}]}\mathbf{J}^{\mathbf{T}}\right)\mathbf{J_H^T} + \mathbf{J_{\bar{f}}}\left(\mathbf{J_Y}\mathbf{\Sigma_Y}\mathbf{J_Y^T} + \mathbf{J_v}\mathbf{\Sigma_v}\mathbf{J_v^T}\right)\mathbf{J_{\bar{f}}^T} \tag{48}$$

with the corresponding Jacobians given by Eqs. ((23), (35), (39), (40) and (46) or (47). Eq. (48) thus summarises the uncertainty framework proposed for a component-based TPA. For a blocked force (or classical) TPA the above is modified to take into account the directly measured forward FRFs $\mathbf{H}$, and their possible correlation with the inverse FRFs $\mathbf{Y}$,

$$\mathbf{\Sigma_p} = \mathbf{J_H}\mathbf{\Sigma_H}\mathbf{J_H^T} + \mathbf{J_{\bar{f}}}\left(\mathbf{J_Y}\mathbf{\Sigma_Y}\mathbf{J_Y^T} + \mathbf{J_v}\mathbf{\Sigma_v}\mathbf{J_v^T}\right)\mathbf{J_{\bar{f}}^T} + \left[\mathbf{J_H}\mathbf{\Sigma_{H,Y}}\mathbf{J_{HY}^T} + \mathbf{J_{HY}}\mathbf{\Sigma_{Y,H}}\mathbf{J_H^T}\right]. \tag{49}$$

with the Jacobian $\mathbf{J_{HY}}$ given by equation (42).

The bivariate covariance matrix $\mathbf{\Sigma_p}$ describes the uncertainty in the real and imaginary components of the TPA response prediction. In practice, however, we are typically more interested in magnitude and phase descriptors.

For small levels of uncertainty, propagation through a TPA may be considered linear and described using the equations derived above. In this case, the distribution of the resulting uncertainty is unchanged, i.e. a Gaussian input uncertainty will yield a Gaussian output uncertainty. The propagation of uncertainty through the magnitude function $|p_i| = \sqrt{\mathrm{Re}(p_i)^2 + \mathrm{Im}(p_i)^2}$,

however, differs in that the magnitude cannot support negative values, and as such its distribution cannot be Gaussian. The magnitude (and phase) distribution of two jointly correlated Gaussian variables (for example, the real and imaginary components of a response prediction p) was derived in Ref. [20]. In the simplified case that the real and imaginary components are uncorrelated and of equal variance, this complex expression reduces to the Rayleigh distribution.

In previous work the authors have used a linear covariance propagation, where the bivariate uncertainty $\mathbf{\Sigma_p}$ is propagated through the magnitude function $|p_i| = \sqrt{\mathrm{Re}(p_i)^2 + \mathrm{Im}(p_i)^2}$, and assigned to an (assumed) log-normal distribution, thus allowing a confidence interval to be estimated [10,13]. This linear covariance propagation is given by the equation [21],

$$\sigma^2_{|p_i|} = \begin{pmatrix} \dfrac{\mathrm{Re}(p_i)}{\sqrt{\mathrm{Re}(p_i)^2 + \mathrm{Im}(p_i)^2}} & \dfrac{\mathrm{Im}(p_i)}{\sqrt{\mathrm{Re}(p_i)^2 + \mathrm{Im}(p_i)^2}} \end{pmatrix} \begin{bmatrix} \sigma_{\mathrm{Re}(p_i)\mathrm{Re}(p_i)} & \sigma_{\mathrm{Re}(p_i)\mathrm{Im}(p_i)} \\ \sigma_{\mathrm{Im}(p_i)\mathrm{Re}(p_i)} & \sigma_{\mathrm{Im}(p_i)\mathrm{Im}(p_i)} \end{bmatrix} \begin{pmatrix} \dfrac{\mathrm{Re}(p_i)}{\sqrt{\mathrm{Re}(p_i)^2 + \mathrm{Im}(p_i)^2}} \\ \dfrac{\mathrm{Im}(p_i)}{\sqrt{\mathrm{Re}(p_i)^2 + \mathrm{Im}(p_i)^2}} \end{pmatrix}. \tag{50}$$

Note that a similar procedure may be used to determine the uncertainty in phase angle, $\angle p_i = \tan^{-1}\left(\frac{\mathrm{Im}(p_i)}{\mathrm{Re}(p_i)}\right)$ [21].

Whilst the log-normal distribution satisfies the non-negative requirement, its agreement with the analytic result can vary greatly depending on the variance, covariance and expected values of the real and imaginary components. An alternative approach will be considered here, based on a Monte-Carlo simulation.

Having estimated the expected value and bivariate covariance matrix of the target quantity, $\mathbb{E}[\mathbf{p}]$ and $\mathbf{\Sigma_p}$, assuming a bivariate normal distribution, a series of N correlated variables can be (randomly) generated. A magnitude confidence interval can then be estimated by taking the magnitude of each correlated pair and inspecting the resultant empirical cumulative density function (ECDF). This approach is more reliable than assuming a log-normal distribution providing that N is chosen to be sufficiently large. An illustrative example is presented in section 4.3.1.

Before proceeding further it is worth considering the limitations of the proposed framework. Eqs. (48) and (49) are based on the linearisation of the TPA equations. In the presence of a non-linear function an approximation is introduced, the accuracy of which worsens for increased input uncertainty. The non-linear elements of Eqs. (48) and (49) are those associated with matrix inversions, namely, the blocked force matrix inversion (i.e. propagating $\mathbf{\Sigma_Y}$ onto $\mathbf{\Sigma_{\tilde{f}}}$) and the DS procedure (i.e. propagating $\mathbf{\Sigma_{[Y]}}$ onto $\mathbf{\Sigma_{Y_c}}$). The propagation of uncertainty through a matrix inversion in the context of a blocked force characterisation and a DS prediction was investigated numerically in Refs. [10,13] for moderate levels of uncertainty, with good agreement obtained against Monte-Carlo (MC) simulations. Nevertheless, in the presence of large input uncertainty, propagation through the non-linear elements of Eqs. (48) and (49) should be performed using a MC method. The resulting MC uncertainties can then be used in place of their linearised counterparts in the above framework. Take for example, the linearised uncertainty propagation $\mathbf{J_Y \Sigma_Y J_Y^T} = \mathbf{\Sigma_{\tilde{f}_{(Y)}}}$, i.e. the propagation of FRF uncertainty onto the blocked force. A simple MC procedure may be outlined as follows:

1) Calculate a set of N of blocked force vectors by randomly sampling from the set of measured FRFs $\mathbf{Y}$.
2) From the N blocked force vectors estimate a bivariate covariance matrix $\mathbf{\Sigma^{(MC)}_{\tilde{f}_{(Y)}}}$.
3) Substitute the MC covariance matrix $\mathbf{\Sigma^{(MC)}_{\tilde{f}_{(Y)}}}$ for the linearised propagation term $\mathbf{J_Y \Sigma_Y J_Y^T}$ in equation (48).

Note that N should be made sufficiently large such that an accurate covariance estimate is obtained. A similar MC procedure may also be required to replace the terms $\left(\mathbf{J\Sigma_{[Y]}J^T}\right)$ and $\left[\mathbf{J_H \Sigma_{H,Y} J_{HY}^T + J_{HY} \Sigma_{Y,H} J_H^T}\right]$, or if a regularised solution is sought, as the derived Jacobians would no longer be appropriate.

Whilst, in theory, the above framework may be extended to include second order derivatives for the non-linear elements, thus improving its accuracy for large input uncertainty (see for example [11]), this is considered beyond the scope of the present paper.

Finally, a unique advantage of the proposed framework is that Eqs. (48) and (49) may be broken down to various degrees and used to access/rank order the uncertainty contributions from each component/test, thus facilitating a benefit analysis (see for example [13]). Similarly, based on the proposed framework the uncertainty in a rank ordering of source contributions can also be assessed. This topic is discussed further in section 5.

4.3.1. Monte-Carlo confidence interval estimation

In this section we will demonstrate the procedure used to estimate the magnitude confidence bounds of a jointly correlated complex quantity.

It is assumed that the expected value $\mathbb{E}[v]$ and bivariate covariance matrix $\mathbf{\Sigma_v}$ of the target quantity v are available. To estimate the magnitude confidence bounds of v an assumption must first be made regarding the distribution of its underlying uncertainty. Here we will assume that $\mathrm{Re}(v)$ and $\mathrm{Im}(v)$ are joint normally distributed with the bivariate covariance matrix,

$$\mathbf{\Sigma_v} = \begin{bmatrix} 1 & 0.55 \\ 0.55 & 1.1 \end{bmatrix}. \tag{51}$$

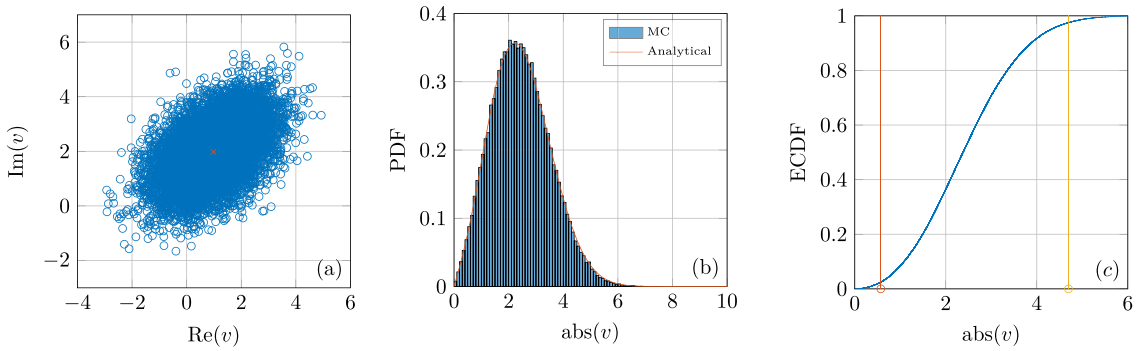

Fig. 2. Example estimation of magnitude confidence interval. (a) - Generate N correlated samples according to $\boldsymbol{\Sigma}_{\mathbf{v}}$ and $\mathbb{E}[v]$. (b) - Take magnitude of all samples to obtained PDF. (c) - Calculate ECDF and find α and $1-\alpha$ values of abs(v).

Note that the same procedure may be used for other assumed distributions.

Based on $\boldsymbol{\Sigma}_{\mathbf{v}}$ and $\mathbb{E}[v] = 1 + 2i$, N random samples are drawn from a bivariate distribution (see Fig. 2a). The magnitude of each sample pair (together representing the complex quantity v) is taken and used to estimate a Probability Distribution Function (PDF), as in Fig. 2b. Also shown in Fig. 2b is the analytic PDF obtained using equation (1) of [20].

From the PDF an Empirical Cumulative Density Function (ECDF) is estimated, as shown in Fig. 2c. The $\pm$95% confidence bounds of $|v|$ are then found by inspecting the values of $|v|$ for which the ECDF is equal to α and $1-\alpha$, where $\alpha = (1-0.95)/2$. For the example considered here these values are 0.57 and 4.7, and are shown by the orange and yellow lines, respectively. For frequency dependent quantities the above procedure is repeated at each frequency interval. The accuracy of the confidence bound estimation will depend on the appropriateness of the assumed bivariate normal distribution, and the number of random samples drawn.

4.4. Estimation of a bivariate covariance matrix

Successful implementation of the above framework relies on first estimating the bivariate covariance matrices, $\boldsymbol{\Sigma}_{\mathbf{v}}$, $\boldsymbol{\Sigma}_{\mathbf{Y}}$, $\boldsymbol{\Sigma}_{\mathbf{H}}$, and $\boldsymbol{\Sigma}_{\mathbf{H,Y}}$. These matrices must be arranged in accordance with the Jacobian matrices derived above so that each variance and covariance element is propagated correctly.

Given a complex response vector $\mathbf{v} \in \mathbb{C}^M$, where each element is measured R_v times, the bivariate covariance matrix $\boldsymbol{\Sigma}_{\mathbf{v}}$ is obtained as follows. Each realisation of the vector is horizontally aligned as,

$$\widehat{\mathbf{v}} = \left[M_v(\mathbf{v}^1) \;\; M_v(\mathbf{v}^2) \;\; \cdots \;\; M_v(\mathbf{v}^{R_v})\right] \tag{52}$$

where the operator $M_v(\;\;)$ is applied element-wise, and defined as

$$M_v(A) = \begin{pmatrix} \mathrm{Re}(A) \\ \mathrm{Im}(A) \end{pmatrix}. \tag{53}$$

The bivariate covariance matrix $\boldsymbol{\Sigma}_{\mathbf{v}}$ is then estimated using the standard formula [22],

$$\boldsymbol{\Sigma}_{\mathbf{v}} = \frac{1}{R-1}\left[\left(\widehat{\mathbf{v}} - \mathbb{E}[\widehat{\mathbf{v}}]\right)\left(\widehat{\mathbf{v}} - \mathbb{E}[\widehat{\mathbf{v}}]\right)^{\mathbf{T}}\right] \tag{54}$$

where the expectation $\mathbb{E}[\;\;]$ (taken along the columns of $\widehat{\mathbf{v}}$) is subtracted from each column of the matrix $\widehat{\mathbf{v}}$.

Similarly, given a complex FRF matrix $\mathbf{Y} \in \mathbb{C}^{M\times N}$ where each element is measured R_Y times, the bivariate covariance matrix may be obtained as follows. Each realisation of the matrix is vectorised, using the operator vec(\;\;), and horizontally aligned as so,

$$\widehat{\mathbf{Y}} = \left[M_v(\mathrm{vec}(\mathbf{Y}^1)) \;\; M_v(\mathrm{vec}(\mathbf{Y}^2)) \;\; \cdots \;\; M_v(\mathrm{vec}(\mathbf{Y}^{R_Y}))\right] \tag{55}$$

where M_v is again applied element-wise. The bivariate covariance matrix $\boldsymbol{\Sigma}_{\mathbf{Y}}$ is then estimated according to Eq. (54). When estimating the bivariate covariance matrix of the uncoupled FRF matrix (for use in DS), Eq. (54) applies to the block diagonalised FRF matrix (i.e. all zero elements are included). Note that the cross-covariance, $\boldsymbol{\Sigma}_{\mathbf{H,Y}}$, is obtained similarly,

$$\boldsymbol{\Sigma}_{\mathbf{H,Y}} = \frac{1}{R-1}\left[\left(\widehat{\mathbf{H}} - \mathbb{E}\left[\widehat{\mathbf{H}}\right]\right)\left(\widehat{\mathbf{Y}} - \mathbb{E}\left[\widehat{\mathbf{Y}}\right]\right)^{\mathbf{T}}\right]. \tag{56}$$

where $\widehat{\mathbf{H}}$ is defined as per Eq. (55). An important feature of the proposed uncertainty framework is that no additional experimental effort is required in obtaining the above covariance matrices, only that repeated measurements are stored individually alongside their computed average.

When estimating the bivariate covariance matrices it is important to consider the existence of a meaningful correlation. In practice only a small number of repeated measurements will be performed, meaning that uncorrelated variables will be left with some non-zero covariance. If the user is confident that this is an artefact of the finite set of measurements, the covariance may be set to 0. If a correlation truly exists however these terms must be retained. For example, the FRF matrix $\mathbf{Y}$ is typically measured one column at a time (i.e. multiple responses due to a shared excitation). Given that they are measured separately, the columns of $\mathbf{Y}$ are uncorrelated with each other and their covariance is 0 [12]. The elements within a given column are however correlated due to their shared excitation. In this case $\boldsymbol{\Sigma}_{\mathbf{Y}}$ would be block diagonal.

It is important to note that Eq. (54) describes the statistical variation between individual samples. Consequently, the proposed framework provides an uncertainty estimate based on the overall spread of samples collected i.e. the variance obtained when randomly choosing individual samples and computing a result. Alternatively, interest may lie in the uncertainty of the expected value. In this case the covariance matrix should be normalised by the number of samples used in its estimation, $\boldsymbol{\Sigma}_{\mathbb{E}[\mathbf{v}]} = \boldsymbol{\Sigma}_{\mathbf{v}}/R_v$, where $\boldsymbol{\Sigma}_{\mathbb{E}[\mathbf{v}]}$ describes the uncertainty in $\mathbb{E}[\mathbf{v}]$. This normalisation does not affect the formulation of the proposed framework, nor any later developments presented in this work.

As a final remark, it should be noted that whilst there exist common statistical error analysis relations for the quantification of uncertainty in measured input/output relations, such as FRFs [23,24], these are not appropriate in the context of the above uncertainty propagation; their formulation is based on the assumption of uncorrelated real and imaginary components with equal variance, and furthermore, does not account for the presence of inter-FRF correlation, which has been shown to be essential in the propagation of uncertainty. It is for this reason that the more general bivariate covariance description described above has been adopted.

5. Uncertainty in contribution analysis and rank ordering

Transfer path analysis may be used as a diagnostic (blocked force TPA) or predictive (component-based TPA) tool. As a predictive tool, concern is placed on accurately predicting the operational response $\mathbf{p}$ based on the measurement of each individual sub-structure. As a diagnostic tool, we are interested in determining the relative contribution of each excitation force to the total operational response. Using this information design engineers are able to identify troublesome contributions and apply appropriate treatments and/or modifications. The uncertainty framework presented thus far provides a means of estimating the uncertainty in the total operational response, i.e. $\boldsymbol{\Sigma}_{\mathbf{p}}$. In this section we will consider the uncertainty in the relative contribution of each excitation, i.e. the uncertainty in rank ordering.

Considering a single response variable p, Eq. (37) may be rewritten in the form,

$$p = \sum_n p_n = \sum_n H_{pn}\bar{f}_n \tag{57}$$

where: p_n represents the response contribution due to the nth blocked force $\bar{f}_n$, and H_{pn} is the nth element of the forward FRF vector $\mathbf{H}$. The contribution magnitudes $|p_n|$ are often rank ordered to identify the most dominant excitation. We are interested in evaluating our confidence in the rank of a given contribution. For example, given the total response p, and the experimental data used to estimate it, we are interested in the probability P( ) that $|p_2|$ (i.e. the second largest contribution) is equal to or greater than $|p_1|$ (i.e the largest contribution), $\mathrm{P}(|p_2| \geq |p_1|)$. More generally we are interested in the probability $\mathrm{P}(|p_i| \geq |p_j|)$, or alternatively, $\mathrm{P}(|p_i| - |p_j| \geq 0)$, where $|p_i|$ is the magnitude of the ith largest contribution.

To simplify the subsequent analysis we will assume that $|p_i|$ and $-|p_j|$ are uncorrelated random variables (RVs), although in reality this may not be the case. The contributions $|p_i|$ and $-|p_j|$ are distributed according to their respective PDFs, $f_i(x)$ and $f_j(x)$. To obtain $\mathrm{P}(|p_i| - |p_j| \geq 0)$, we begin by noting that the sum of two (arbitrary) RVs returns another RV whose PDF is given by the convolution of their respective PDFs,

$$f_{i+j}(x) = \int_{-\infty}^{+\infty} f_i(x-t)f_j(t)\mathrm{d}t. \tag{58}$$

That is, $|p_i| - |p_j|$ is distributed according to $f_{i+j}(x)$. Similarly, for discrete variables,

$$\mathrm{P}(|p_i| - |p_j| = x) = \sum_{k=-\infty}^{\infty} \mathrm{P}(|p_i| = k)\mathrm{P}(-|p_j| = x-k). \tag{59}$$

The probability that $|p_i| - |p_j| \geq 0$, can then be obtained by integrating over $x \geq 0$,

$$\mathrm{P}(|p_i| - |p_j| \geq 0) = \int_0^{\infty} f_{i+j}(x)\mathrm{d}x = \int_0^{\infty} \int_{-\infty}^{\infty} f_i(x-t)f_j(t)\mathrm{d}t\mathrm{d}x. \tag{60}$$

Or in the discrete variable case,

$$\mathrm{P}(|p_i| - |p_j| \geq 0) = \sum_{x=0}^{\infty} \mathrm{P}(|p_i| - |p_j| = x) = \sum_{x=0}^{\infty} \sum_{k=-\infty}^{\infty} \mathrm{P}(|p_i| = k)\mathrm{P}(-|p_j| = x-k). \tag{61}$$

To evaluate $\mathrm{P}(|p_i| - |p_j| \geq 0)$ the PDFs $f_i(x)$ and $f_j(x)$ must first be computed. Although analytical expressions exist for these distributions (see Ref. [20]), the numerical complexity and additional effort required to compute $\mathrm{P}(|p_i| - |p_j| \geq 0)$ analytically

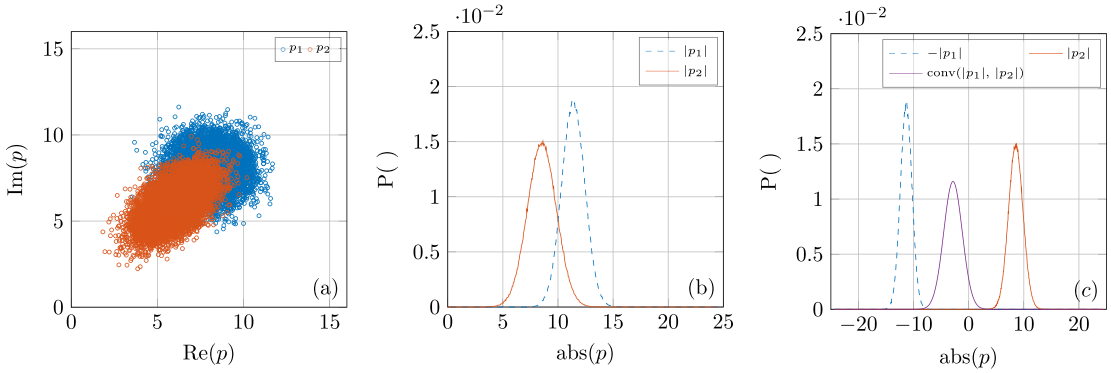

Fig. 3. Steps for computing the probability of an incorrect rank ordering. (a) - Generate random samples. (b) - Compute PDFs of absolute values. (c) - Convolve to obtain PDF of P($|p_2| - |p_1|$).

renders a Monte-Carlo (MC) approach more convenient. Using $\mathbb{E}[p_i]$, $\mathbb{E}[p_j]$, $\mathbf{\Sigma_{p_i}}$ and $\mathbf{\Sigma_{p_j}}$, random samples are drawn according to an assumed bivariate normal distribution. The PDFs $f_i(x)$ and $f_j(x)$ are then estimated and convolved prior to a numerical integration. These steps are illustrated in Fig. 3. Note that the same procedure may be used for other assumed distributions.

Shown in Fig. 3a are the random samples drawn for the response contributions p_1 and p_2, based on their expectations, $\mathbb{E}[p_1]$ and $\mathbb{E}[p_2]$, and their bivariate covariance matrices, $\mathbf{\Sigma_{p_1}}$ and $\mathbf{\Sigma_{p_2}}$. For the example considered $\mathbb{E}[|p_1|] > \mathbb{E}[|p_2|]$. We are interested in P($|p_2| - |p_1| \geq 0$), i.e. the probability of $|p_2|$ exceeding $|p_1|$. The absolute value is taken of each sample and the PDFs of $|p_1|$ and $|p_2|$ are estimated, as illustrated in Fig. 3b. The PDF of $|p_2| - |p_1|$ is then computed by convolving those of Fig. 3b (making sure to negate that of $|p_1|$). The resulting PDF is shown in Fig. 3c in purple. The probability P($|p_2| - |p_1| \geq 0$) is then obtained by summing over the positive x-axis. In this example P($|p_2| \geq |p_1|$) $\approx$ 0.05.

To apply the above method the expectations and bivariate covariance matrices of the two contributions being analysed are required. The expectation $\mathbb{E}[p_i]$ is obtained by simply setting all blocked force elements, bar the ith entry, to zero, and calculating the resulting response. Similarly, $\mathbf{\Sigma_{p_i}}$ may be obtained by setting all entries of $\mathbf{\Sigma_{\bar{f}}}$ not associated with the blocked force element $\bar{f}_i$ to zero and performing the uncertainty propagation with the remaining elements.

6. Condition number as an indicator of uncertainty

It is common practice when analysing dynamic systems to associate the condition number of the system matrix ($\mathbf{Y}$) with the level of uncertainty, or error, present in the solution of an inverse problem. In this section we will briefly discuss the condition number, in the context of uncertainty propagation, and investigate its relation to the proposed framework.

We begin by recalling Eq. (2),

$$\mathbf{v} = \mathbf{Y}\bar{\mathbf{f}} \tag{62}$$

omitting subscripts for clarity. For simplicity we will consider the case that the system matrix is square. The solution (i.e. the blocked force vector $\bar{\mathbf{f}}$) is then obtained using the conventional matrix inverse,

$$\bar{\mathbf{f}} = \mathbf{Y}^{-1}\mathbf{v}. \tag{63}$$

The condition number $\kappa(\mathbf{Y})$ can be defined as the (maximum) ratio of the relative error in the output (i.e. $\bar{\mathbf{f}}$) for a relative error on the input (i.e. $\mathbf{v}$) or the system matrix (i.e $\mathbf{Y}$), in a normed sense [25],

$$\kappa(\mathbf{Y}) = \max\left\{\left(\frac{\|\mathrm{d}(\bar{\mathbf{f}})\|}{\|\bar{\mathbf{f}}\|}\right)\left(\frac{\|\mathbf{v}\|}{\|\mathrm{d}(\mathbf{v})\|}\right)\right\} \quad \text{or} \quad \max\left\{\left(\frac{\|\mathrm{d}(\bar{\mathbf{f}})\|}{\|\bar{\mathbf{f}}\|}\right)\left(\frac{\|\mathbf{Y}\|}{\|\mathrm{d}(\mathbf{Y})\|}\right)\right\}, \tag{64}$$

where $\|\quad\|$ is used to represent any consistent norm. Recalling from section 4.2.1 the differential blocked force $\mathrm{d}(\bar{\mathbf{f}})$,

$$\mathrm{d}\bar{\mathbf{f}} = -(\mathbf{Y}^{-1}\mathbf{v})^{\mathbf{T}} \otimes \mathbf{Y}^{-1}\mathrm{vec}(\mathrm{d}\mathbf{Y}) + \mathbf{Y}^{-1}\mathrm{d}\mathbf{v} \tag{65}$$

it is straight forward to show that when considering a perturbation on the system's input (i.e. the differential velocity term $\mathrm{d}\mathbf{v}$), equation (64) reduces to the well known form [25],

$$\kappa(\mathbf{Y}) = \max\left\{\frac{\|\mathbf{Y}^{-1}\mathrm{d}\mathbf{v}\|}{\|\bar{\mathbf{f}}\|}\frac{\|\mathbf{Y}\bar{\mathbf{f}}\|}{\|\mathrm{d}\mathbf{v}\|}\right\} = \frac{\|\mathbf{Y}^{-1}\| \cdot \|\mathrm{d}\mathbf{v}\|}{\|\bar{\mathbf{f}}\|}\frac{\|\mathbf{Y}\| \cdot \|\bar{\mathbf{f}}\|}{\|\mathrm{d}\mathbf{v}\|} = \|\mathbf{Y}^{-1}\| \cdot \|\mathbf{Y}\|, \tag{66}$$

and that the same result is obtained if one similarly considers a perturbation on the system matrix (i.e. the differential FRF term d$\mathbf{Y}$); the condition number is valid for a perturbation on either the system's matrix or input.

It is important to note that in deriving the condition number the differential terms d$\mathbf{v}$ and d$\mathbf{Y}$ are lost through cancellation. That is to say, the condition number does not take into account the amount of the error present, only its relative amplification (in a normed sense).

In the presence of a uniform input uncertainty (e.g. due to numerical precision, or a bias error), the condition number can be expected to correctly indicate regions of greater uncertainty in an output. In an experimental context, however, the level of input uncertainty will generally vary with frequency. This limits the use of the condition number as an indicator of output uncertainty, particularly as large condition numbers tend to coincide with low levels of input uncertainty.

In the presence of a single dominant mode a high condition number is generally expected since all DoFs are constrained to move according to the mode shape. Yet, at resonance the response and FRF magnitudes reach a local maximum, and so a large signal to noise ratio is achieved (i.e. minimal measurement uncertainty). Furthermore, the natural frequencies of a linear system are inherently stable and do not vary with excitation position, and so the influence of operator uncertainty is also at a minimum. The condition number, therefore, does not reliably estimate which regions of an output are subject to greater uncertainty. In contrast, the uncertainty framework proposed herein takes into account not only the amplification of uncertainty (described by the Jacobian matrix), but the amount of uncertainty present (described by the input covariance matrix).

Although unable to accurately estimate the influence of measurement/operator uncertainty on an acquired blocked force, the condition number may prove useful in identifying regions that are more susceptible to bias errors, e.g. due to model uncertainties.

It is interesting to note that the condition number can also be derived in terms of the uncertainty framework proposed above. Consider the square-root of the maximum ratio of the normed output to input relative covariance matrices,

$$\max\left\{\frac{\|\boldsymbol{\Sigma}_{\bar{\mathbf{f}}}\|}{\|\mathbb{E}[\bar{\mathbf{f}}\bar{\mathbf{f}}^{\mathbf{T}}]\|}\frac{\|\mathbb{E}[\mathbf{v}\mathbf{v}^{\mathbf{T}}]\|}{\|\boldsymbol{\Sigma}_{\mathbf{v}}\|}\right\}^{1/2}. \tag{67}$$

Substituting the blocked force covariance matrix from equation (19) (considering only the operational response covariance) alongside $\mathbf{v}=\mathbf{Y}\bar{\mathbf{f}}$ yields,

$$\max\left\{\frac{\|\mathbf{J}_{\mathbf{v}}\boldsymbol{\Sigma}_{\mathbf{v}}\mathbf{J}_{\mathbf{v}}^{\mathbf{T}}\|}{\|\mathbb{E}[\bar{\mathbf{f}}\bar{\mathbf{f}}^{\mathbf{T}}]\|}\frac{\|\mathbb{E}[\mathbf{Y}\bar{\mathbf{f}}\bar{\mathbf{f}}^{\mathbf{T}}\mathbf{Y}^{\mathbf{T}}]\|}{\|\boldsymbol{\Sigma}_{\mathbf{v}}\|}\right\}^{1/2}. \tag{68}$$

Applying the Cauchy–Schwarz inequality, $\|AB\| \leq \|A\|\cdot\|B\|$, and taking the upper limit, yields the maximum value,

$$\left[\frac{\|\mathbf{J}_{\mathbf{v}}\|\cdot\|\boldsymbol{\Sigma}_{\mathbf{v}}\|\cdot\|\mathbf{J}_{\mathbf{v}}^{\mathbf{T}}\|}{\|\mathbb{E}[\bar{\mathbf{f}}\bar{\mathbf{f}}^{\mathbf{T}}]\|}\frac{\|\mathbb{E}[\mathbf{Y}]\|\cdot\|\mathbb{E}[\bar{\mathbf{f}}\bar{\mathbf{f}}^{\mathbf{T}}]\|\cdot\|\mathbb{E}[\mathbf{Y}^{\mathbf{T}}]\|}{\|\boldsymbol{\Sigma}_{\mathbf{v}}\|}\right]^{1/2} = \left[\|\mathbf{J}_{\mathbf{v}}\|\cdot\|\mathbf{J}_{\mathbf{v}}^{\mathbf{T}}\|\cdot\|\mathbb{E}[\mathbf{Y}]\|\cdot\|\mathbb{E}[\mathbf{Y}^{\mathbf{T}}]\|\right]^{1/2} = \|\mathbf{J}_{\mathbf{v}}\|\cdot\|\mathbb{E}[\mathbf{Y}]\|. \tag{69}$$

Recalling the Jacobian matrix from section 4.2.1 (omitting the complex matrix mapping operator), the above becomes,

$$\|\mathbf{J}_{\mathbf{v}}\|\cdot\|\mathbb{E}[\mathbf{Y}]\| = \|\mathbb{E}[\mathbf{Y}^{-\mathbf{1}}]\|\cdot\|\mathbb{E}[\mathbf{Y}]\| \quad \text{or} \quad \|\mathbb{E}[\mathbf{J}_{\mathbf{v}}]\|\cdot\|\mathbb{E}[\mathbf{J}_{\mathbf{v}}^{-\mathbf{1}}]\|. \tag{70}$$

This is in agreement with the standard definition of condition number. It is straightforward to show that the same result is obtained if the FRF covariance matrix were considered instead. Hence the condition number may interpreted as a ratio of the output to input relative covariance and expressed in terms of the Jacobian matrices derived above,

$$\kappa(\mathbf{Y}) = \|\mathbf{J}_{\mathbf{v}}^{-\mathbf{1}}\|\cdot\|\mathbf{J}_{\mathbf{v}}\| \quad \text{or} \quad \|\mathbf{J}_{\mathbf{Y}}^{-\mathbf{1}}\|\cdot\|\mathbf{J}_{\mathbf{Y}}\|. \tag{71}$$

In summary, the condition number may be interpreted as a single number value for the amplification of relative covariance between the input and output variables, in a normed sense. The condition number does not acknowledge the level of uncertainty (or error) in either the system's matrix or input, nor any correlations present. Whilst the condition number may be expressed in terms of the Jacobian matrices used in the propagation of uncertainty, it provides only a condensed single value description of the system's sensitivity to error. In contrast, the Jacobians used in the proposed framework describe with great detail the sensitivity of each output variable to each input variable. Furthermore, the proposed framework, unlike the condition number, considers the amount of uncertainty in the system's matrix and input. This is particularly important as regions of large condition number (e.g. at resonance) do not tend to coincide with regions of large input uncertainty [10].

7. A note on model uncertainties

The uncertainty propagation framework presented thus far has considered only the random uncertainties present in the measured FRFs and operational responses, i.e. experimental and source based uncertainty. As discussed in section 1 however, there exists an additional source of uncertainty, emanating from the use of an approximate model to describe the physical assembly. Strictly speaking, this form of 'model uncertainty' introduces a systematic/bias error as opposed to random uncertainty. Nevertheless, model uncertainty is an important source of error in TPA, and thus warrants a brief discussion with regards its most likely origin. Furthermore, the proposed uncertainty framework is formulated under the assumption that no significant bias errors are present, and so the reader should be made aware of how to detect/avoid such errors. A more detailed discussion

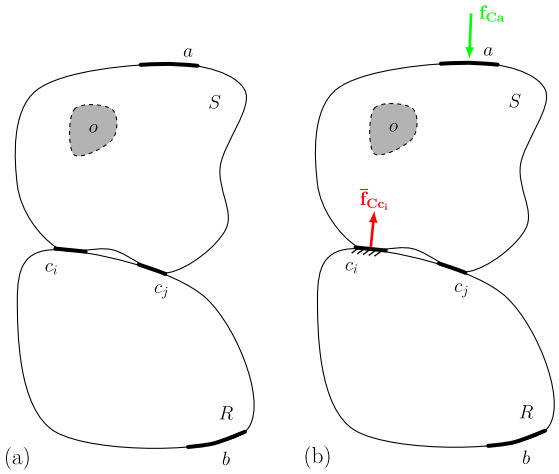

Fig. 4. Constrained (a) and unconstrained (b) source-receiver assemblies.

of model uncertainty and its underlying causes (incompleteness and inconsistency) can be found in Refs. [26,27]. For completeness, key details will be summarised below.

7.1. Completeness

Completeness describes the degree to which an interface has been correctly represented. For example, whether enough DoFs have been included (i.e. rotations/in-plane). Take for example the assembly in Fig. 4, where a source and receiver are coupled via two sets of DoFs, c_i and c_j. Suppose the DoFs c_j are unknown, or known but cannot be measured (e.g. rotational DoFs). It is straight forward to show that a characterisation of the blocked force at the remaining c_i DoFs (i.e. neglecting those at c_j) leads to [27,28],

$$\widetilde{\bar{\mathbf{f}}}_{\mathbf{Cc_i}} = \mathbf{f}_{\mathbf{Sc_i}} + \mathbf{Y}^{-1}_{\mathbf{Cbc_i}} \mathbf{Y}_{\mathbf{Cbc_j}} \bar{\mathbf{f}}_{\mathbf{Sc_j}} \tag{72}$$

where: $\widetilde{\bar{\mathbf{f}}}_{\mathbf{Cc_i}}$ is the acquired blocked force at the DoFs c_i, $\bar{\mathbf{f}}_{\mathbf{Sc_i}}$ is the true blocked force at the DoFs c_i, and $\mathbf{Y}^{-1}_{\mathbf{Cbc_i}} \mathbf{Y}_{\mathbf{Cbc_j}} \bar{\mathbf{f}}_{\mathbf{Sc_j}}$ is an additional term due to the neglected DoFs c_j (i.e. incompleteness). Note that, due to this addition term, the acquired blocked force is a property of the coupled assembly, not the source. When used to predict an operational response (either in the same assembly, as in a blocked force TPA, or in a new assembly, as in a component-based TPA), this additional term will introduce a bias error.

When characterising an active component in terms of its blocked force it is important to minimise the effect of bias errors due to neglected DoFs. With this in mind, Meggitt et al. [27,28] proposed an Interface Completeness Criterion (ICC). Based on measurements conducted during a standard in-situ blocked force characterisation, the ICC provides a quantitative assessment of the degree to which an interface has been completely defined. The ICC is derived by considering an assembly whose known DoFs are mathematically blocked (see Fig. 4b). In this constrained assembly, transmission between remote source (a) and receiver (b) side DoFs can only occur through the unknown interface DoFs (c_j). Based on this notion the ICC is defined as [27,28],

$$\mathrm{ICC}_{\mathbf{ba}} = \frac{\left| \mathbf{Y}_{\mathbf{Cba}} \left(\mathbf{Y}^{(\mathbf{c_i})}_{\mathbf{Cba}} \right)^H \right|^2}{\mathbf{Y}_{\mathbf{Cba}} \left(\mathbf{Y}_{\mathbf{Cba}} \right)^H \mathbf{Y}^{(\mathbf{c_i})}_{\mathbf{Cba}} \left(\mathbf{Y}^{(\mathbf{c_i})}_{\mathbf{Cba}} \right)^H} \tag{73}$$

where,

$$\mathbf{Y}^{(\mathbf{c_i})}_{\mathbf{Cba}} = \mathbf{Y}_{\mathbf{Cbc_i}} \mathbf{Y}^{-1}_{\mathbf{Cc_ic_i}} \mathbf{Y}_{\mathbf{Cc_ia}}. \tag{74}$$

In the above, $\mathbf{Y}_{\mathbf{Cba}}$ is a vector of coupled FRFs measured between a set of remote source side DoFs a and a single receiver DoF b. $\mathbf{Y}^{(\mathbf{c_i})}_{\mathbf{Cba}}$ is an equivalent vector of FRFs that have been predicted by considering only the known interface DoFs c_i (i.e. neglecting the unknown DoFs c_j). In the case that the interface is fully defined (i.e. $|c_j| = 0$), $\mathbf{Y}^{(\mathbf{c_i})}_{\mathbf{Cba}} = \mathbf{Y}_{\mathbf{Cba}}$ and the ICC is equal to 1. Similarly, in the case that no interface DoFs are considered (i.e. $|c_i| = 0$) the ICC is undefined. If multiple receiver side DoFs are considered, the FRFs $\mathbf{Y}_{\mathbf{Cba}}$ and $\mathbf{Y}^{(\mathbf{c_i})}_{\mathbf{Cba}}$ can be vectorised appropriately and an overall ICC computed [27].

Based on the ICC one can infer the quality of an acquired blocked force; the greater the ICC, the smaller the influence of model uncertainty, and the more reliable the blocked force. Applications of the ICC in this context can be found in Refs. [28–30].

Table 1
Geometric and material properties used in the numerical simulation, where l × w × h are the sub-structure dimensions, E is Young's modulus, ρ is density, ν is Poisson's ratio and η is loss factor.

Sub-structure	l × w × h (m)	E (GPa)	ρ (kg/m^3)	ν (−)	η(−)
Source	0.51 × 0.33 × 0.0015	69	2700	0.3	0.05
Receiver 1	1 × 1.3 × 0.005	3.2	1163	0.3	0.1
Receiver 2	0.8 × 0.6 × 0.005	3.2	1163	0.3	0.1

7.2. Consistency

Consistency relates to a compatibility between the underlying dynamics shared by the active and passive properties of an assembly (or component). Take for example the prediction of an operational response based on a measured blocked force,

$$\mathbf{v_{Cr}} = \mathbf{Y_{Crc}}\widetilde{\bar{\mathbf{f}}}_{\mathbf{Sc}}. \tag{75}$$

In the case of a blocked force TPA, the blocked force $\widetilde{\bar{\mathbf{f}}}_{\mathbf{Sc}}$ is obtained from the same assembly in which a prediction is made. Substituting the blocked force for its inverse calculation,

$$\mathbf{v_{Cr}} = \mathbf{Y_{Crc}}\mathbf{Y}_{\mathbf{Ccc}}^{-1}\mathbf{v_{Cc}} \tag{76}$$

and noting that the operational velocity $\mathbf{v_{Cc}}$ may be expressed in terms of the true blocked force $\bar{\mathbf{f}}_{\mathbf{Sc}}$, Eq. (75) may be rewritten in the form,

$$\mathbf{v_{Cr}} = \mathbf{Y}_{\mathbf{Crc}}^{\mathbf{m}}\left(\mathbf{Y}_{\mathbf{Ccc}}^{\mathbf{m}}\right)^{-1}\left(\mathbf{Y_{Ccc}}\bar{\mathbf{f}}_{\mathbf{Sc}}\right)^{\mathbf{m}} \tag{77}$$

where the superscript $^{\mathbf{m}}$ has been introduced to denote a measured quantity. From the above it is clear that the prediction of $\mathbf{v_{Cr}}$ relies on the successful cancellation of $\mathbf{Y_{Ccc}}$. Note however, the right most $\mathbf{Y_{Ccc}}$ is 'contained within' the operational velocity $\mathbf{v_{Cc}}$.

Suppose that during the operational measurement of $\mathbf{v_{Cc}}$ the passive properties of the structure are altered, for example a small shift in the frequency of a resonance (or anti-resonance), perhaps due to a change in temperature or load. In this case the two $\mathbf{Y_{Ccc}}$ terms in Eq. (77) will correspond to different assembly states, and a perfect cancellation will not be achieved. This inconsistency will introduce a bias error in the operational response prediction. Ideally, it would be possible to quantify the degree of inconsistency through a metric similar to the ICC described above. However, this problem is subject to further investigation.

In summary, to minimise the effect of bias errors sufficient levels of completeness and consistency should be achieved. In the presence of large bias errors, the proposed uncertainty framework may yield in accurate uncertainty estimates.

8. Numerical case study

In this section we will demonstrate the proposed uncertainty framework through a two-part numerical example. In part one a blocked force TPA is considered, where the blocked force is obtained using the in-situ method and used to predict an 'operational' response in a coupled receiver structure. In part two a component-based TPA is considered, where the blocked force obtained from part one is used to predict the operational response in a new assembly, obtained using dynamic sub-structuring.

The assemblies considered each comprise two simply supported plates rigidly coupled at four DoFs. The plates are modelled using the Lagrange-Rayleigh-Ritz approach with sine-sine basis functions [31]. Material properties and sub-structure geometries are detailed in Table 1.

8.1. Blocked force TPA

Shown in Fig. 5 is a diagrammatic illustration of the numerical example considered here. A source plate (in blue) is coupled to a receiver plate (in green) through four rigid elements where, for simplicity, only vertical z translations are considered. We are interested in determining the blocked force at the interface DoFs c, and the uncertainties thereof, based on simulated 'measurements' of the FRF $\mathbf{Y_{Ccc}} \in \mathbb{C}^{4\times4}$ and the operational velocity $\mathbf{v_{Cc}} \in \mathbb{C}^4$,

$$\bar{\mathbf{f}}_{\mathbf{Sc}} = \mathbf{Y}_{\mathbf{Ccc}}^{-1}\mathbf{v_{Cc}}. \tag{78}$$

The operational velocity $\mathbf{v_{Cc}}$ is determined by considering a unit excitation at the internal source DoF a, i.e. $\mathbf{v_{Cc}} = \mathbf{Y_{Cca}} \in \mathbb{C}^4$. The blocked force $\bar{\mathbf{f}}_{\mathbf{Sc}} \in \mathbb{C}^4$ will then be used to predict an operational response in the receiver at a remote DoF b using the FRF $\mathbf{H_{Cbc}} \in \mathbb{C}^{1\times4}$ (the reciprocal case $\mathbf{H_{Cbc}} = \mathbf{H}_{\mathbf{Ccb}}^{\mathbf{T}}$ will also be considered),

$$\mathbf{v_{Cb}} = \mathbf{H_{Cbc}}\bar{\mathbf{f}}_{\mathbf{Sc}}. \tag{79}$$

Note that $\mathbf{H_{Cbc}}$ will be used in place of $\mathbf{Y_{Cbc}}$ to avoid confusion between the forward and inverse FRFs.

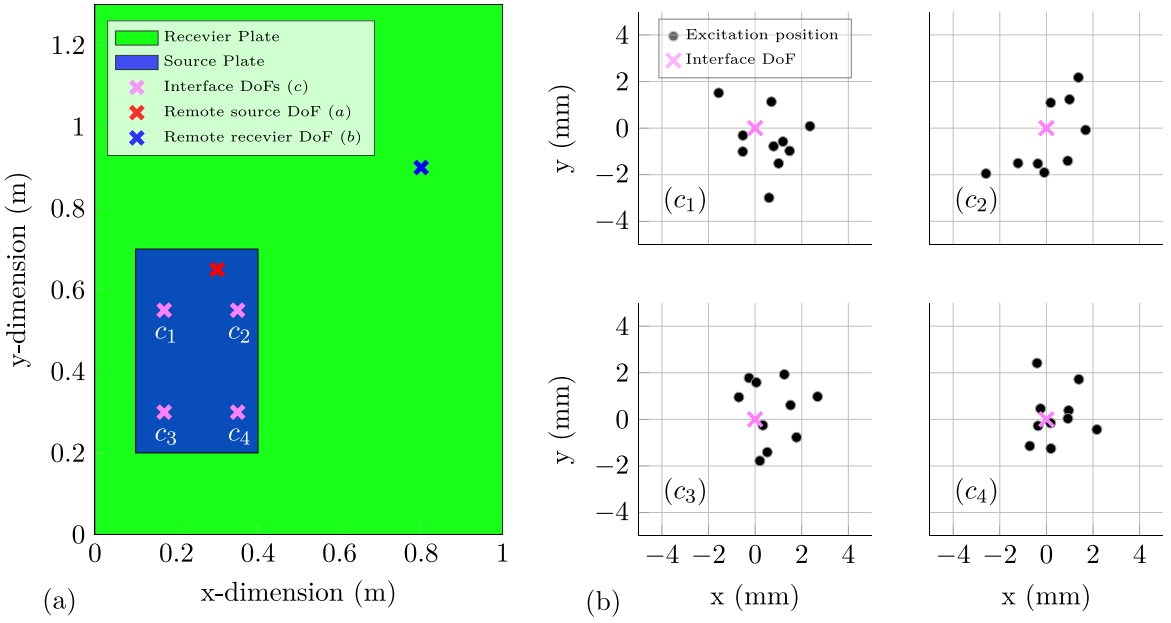

Fig. 5. Diagrammatic illustration of numerical blocked force TPA. (a) - Coupled assembly. (b) - Excitation distribution at each interface DoF.

Uncertainties in the inverse and forward FRFs, $\mathbf{Y}_{\mathbf{Ccc}}$ and $\mathbf{H}_{\mathbf{Cbc}}$, are modelled by randomly distributing their excitation positions according to a bivariate Gaussian distribution, as illustrated in Fig. 5b. This simulates the effect of operator uncertainty (for clarity measurement uncertainty is not considered in the FRFs). Ten random excitations are performed at each interface DoF. Uncertainty in the operational velocity $\mathbf{v}_{\mathbf{Cc}}$ is modelled by adding uncorrelated noise at a specified Signal to Noise Ratio (SNR). This simulates the effect of both measurement and source uncertainty. Fifty independent velocity 'measurements' are obtained this way.

For the blocked force TPA, two cases will be considered. In the first, the forward FRF $\mathbf{H}_{\mathbf{Cbc}}$ is measured reciprocally, thus ensuring its independence from $\mathbf{Y}_{\mathbf{Ccc}}$ (i.e. $\mathbf{H}^{\mathbf{T}}_{\mathbf{Ccb}}$ and $\mathbf{Y}_{\mathbf{Ccc}}$ do not share excitations). Note that when using reciprocal measurements, it is assumed that the error related to inaccurate reciprocal conditions may be considered negligible. In the second case, the forward FRF $\mathbf{H}_{\mathbf{Cbc}}$ is measured simultaneously to $\mathbf{Y}_{\mathbf{Ccc}}$ through a shared excitation, thus ensuring their correlation. These two cases will highlight the importance of the additional covariance terms in Eq. (41).

Shown in Fig. 6 are some illustrative examples of the simulated measurements with their corresponding uncertainties (for clarity these are shown as max/min bounds). The level of operator uncertainty is set by the standard deviation of the excitation distribution. For the blocked force TPA measurements, $\sigma = 0.0013$, which corresponds, roughly, to an excitation within ± 0.25 cm of the indented position, 95% of the time (see Fig. 5b). The operational velocity was assigned an SNR of 15 dB. It is interesting to note that the severity of the operator uncertainty generally increases with frequency. This is due to the greater sensitivity of anti-resonance positioning with a decrease in wavelength. Similar effects are often observed in practice.

Based on the simulated measurements described above, the bivariate covariance matrices $\mathbf{\Sigma}_{\mathbf{Y}} \in \mathbb{R}^{32\times32}$, $\mathbf{\Sigma}_{\mathbf{v}} \in \mathbb{R}^{8\times8}$, $\mathbf{\Sigma}_{\mathbf{H}} \in \mathbb{R}^{8\times8}$, and $\mathbf{\Sigma}_{\mathbf{H,Y}} \in \mathbb{R}^{8\times32}$ are estimated, as per section 4.4. Also calculated are the expectations $\mathbb{E}\left[\mathbf{Y}_{\mathbf{Ccc}}\right] \in \mathbb{C}^{4\times4}$, $\mathbb{E}\left[\mathbf{v}_{\mathbf{Cc}}\right] \in \mathbb{C}^{4}$ and $\mathbb{E}\left[\mathbf{H}_{\mathbf{Cbc}}\right] \in \mathbb{C}^{1\times4}$. These expectations are used to construct the necessary Jacobians, as per section 4.

The inverse propagation of uncertainty is composed of two terms (see Eq. (19)), one related to the FRF uncertainty, and the other to the velocity uncertainty. To validate the proposed framework these terms are separated and compared independently against Monte-Carlo (MC) simulations (this is possible as they are uncorrelated).

Shown in Fig. 7 are the bivariate uncertainties of the blocked force element $\bar{f}_{S_1}$ due to the velocity uncertainty $\mathbf{\Sigma}_{\mathbf{v}}$ only. From top to bottom each plot corresponds to; RelVar $\left[\mathrm{Re}\left(\bar{f}_{S_1}\right)\right]$, RelVar $\left[\mathrm{Im}\left(\bar{f}_{S_1}\right)\right]$ and RelCov $\left[\mathrm{Re}\left(\bar{f}_{S_1}\right), \mathrm{Im}\left(\bar{f}_{S_1}\right)\right]$, where the relative variance and covariance are defined as so,

$$\mathrm{RelVar}\left[A\right] = \frac{\mathrm{Var}[A]}{\mathbb{E}[A]^2} \tag{80}$$

$$\mathrm{RelCov}\left[A, B\right] = \frac{\mathrm{Cov}[A, B]}{\mathbb{E}[A]\mathbb{E}[B]}. \tag{81}$$

In blue are the results obtained from a MC propagation, where the blocked force due to each velocity measurement (of which there were fifty) is calculated. In orange are the results of the proposed framework (referred to as LP, for linear propagation, in all figure legends hereafter). The two are in excellent agreement. This is expected as the velocity's contribution to the blocked

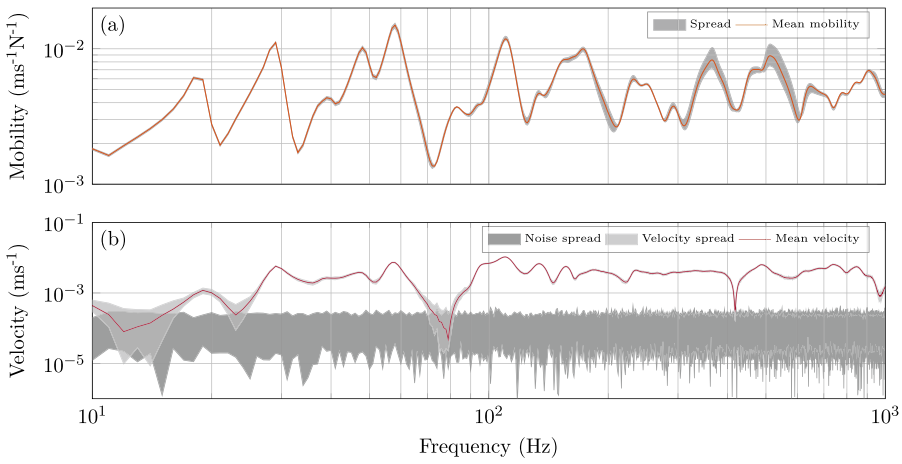

Fig. 6. Examples of simulated uncertainty for the mobility (a) and velocity (b). Operator uncertainty (mobility) was set to $\sigma = 0.0013$. Signal to Noise Ratio (velocity) was set to 15 dB.

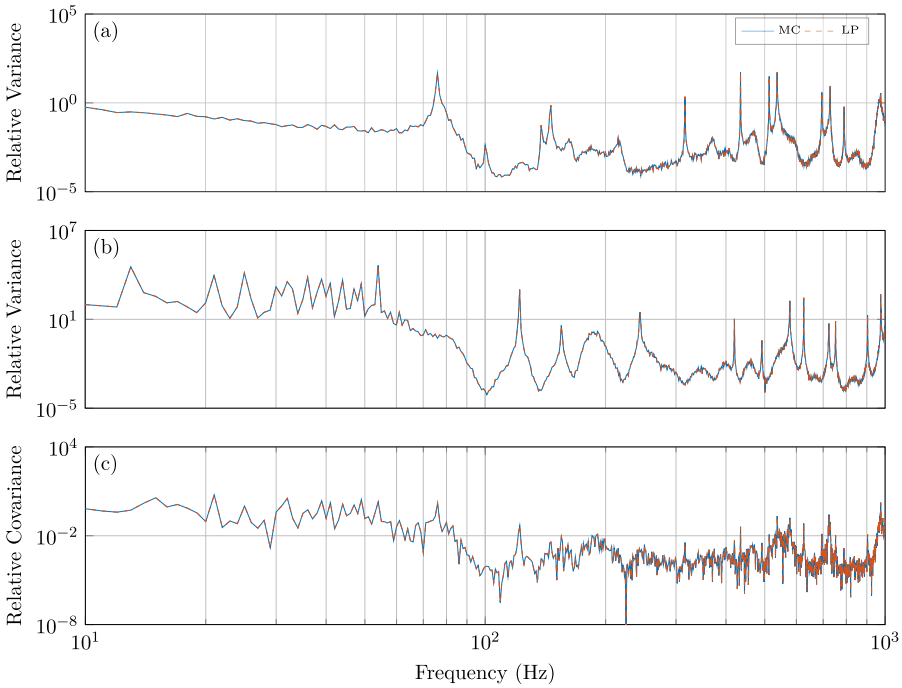

Fig. 7. Bivariate uncertainty in the blocked force $\bar{f}_{S_1}$, due to the velocity uncertainty $\mathbf{\Sigma_v}$ only, predicted using the LP framework (orange) and a MC propagation (blue). Signal to Noise Ratio (SNR) was set to 15 dB. (a) - RelVar $[\mathrm{Re}\,(\bar{f}_{S_1})]$, (b) - RelVar $[\mathrm{Im}\,(\bar{f}_{S_1})]$, (c) - RelCov $[\mathrm{Re}\,(\bar{f}_{S_1})\,, \mathrm{Im}\,(\bar{f}_{S_1})]$. (For interpretation of the references to colour in this figure legend, the reader is referred to the Web version of this article.)

force uncertainty is linear. As such, there are no higher order derivatives and the Jacobian provides an exact propagation.

Shown in Fig. 8 are the bivariate uncertainties of the blocked force element $\bar{f}_{S_1}$ due to the FRF uncertainty $\mathbf{\Sigma_Y}$ only. Unlike Fig. 7 exact agreement is not obtained here, nor is it expected. The FRF's contribution to the blocked force uncertainty is non-linear and therefore subject to some approximation. Nevertheless, for the level of uncertainty considered here (greater than what would typically be expected experimentally), the proposed framework is in good agreement with the MC propagation. A similar level of agreement was obtained for all other $\mathbf{\Sigma_{\bar{f}}}$ elements. Note that a more accurate excitation distribution (i.e. a lower level of uncertainty) would yield better agreement. Likewise, a less accurate excitation distribution would yield poorer agreement.

It is important to note that the results presented in Fig. 8 were obtained by taking the FRF covariance matrix, $\mathbf{\Sigma_Y}$, and setting all uncorrelated elements to 0, i.e. block diagonalising $\mathbf{\Sigma_Y}$ with a 4×4 structure; under the assumption of operator uncertainty

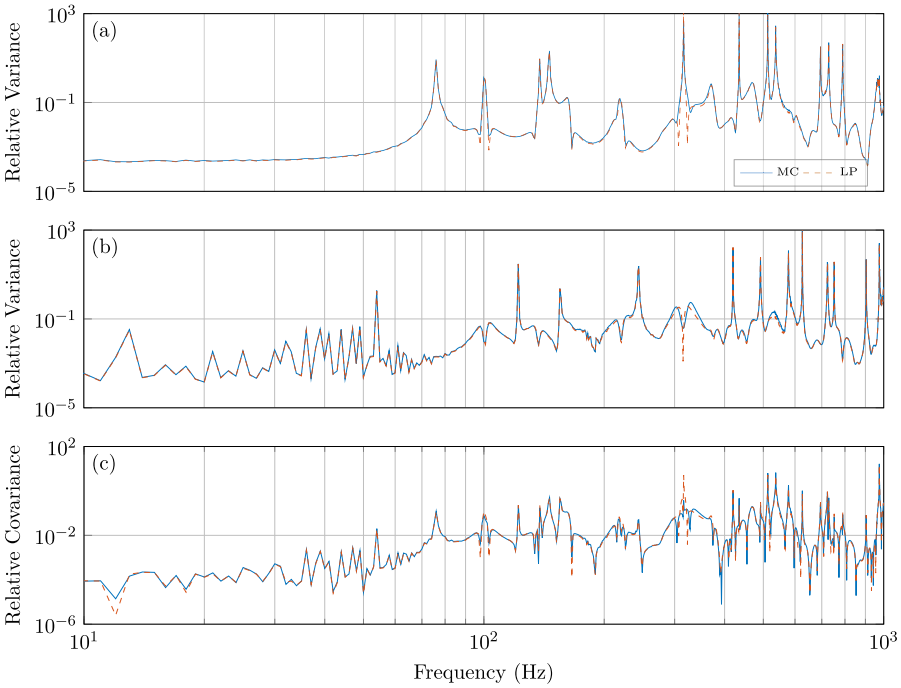

Fig. 8. Bivariate uncertainty in the blocked force $\bar{f}_{S_1}$, due to the mobility uncertainty $\mathbf{\Sigma_Y}$ only, predicted using the LP framework (orange) and a MC propagation (blue). Operator uncertainty was set at $\sigma = 0.0013$. (a) - RelVar $\left[\mathrm{Re}\left(\bar{f}_{S_1}\right)\right]$, (b) - RelVar $\left[\mathrm{Im}\left(\bar{f}_{S_1}\right)\right]$, (c) - RelCov $\left[\mathrm{Re}\left(\bar{f}_{S_1}\right), \mathrm{Im}\left(\bar{f}_{S_1}\right)\right]$.

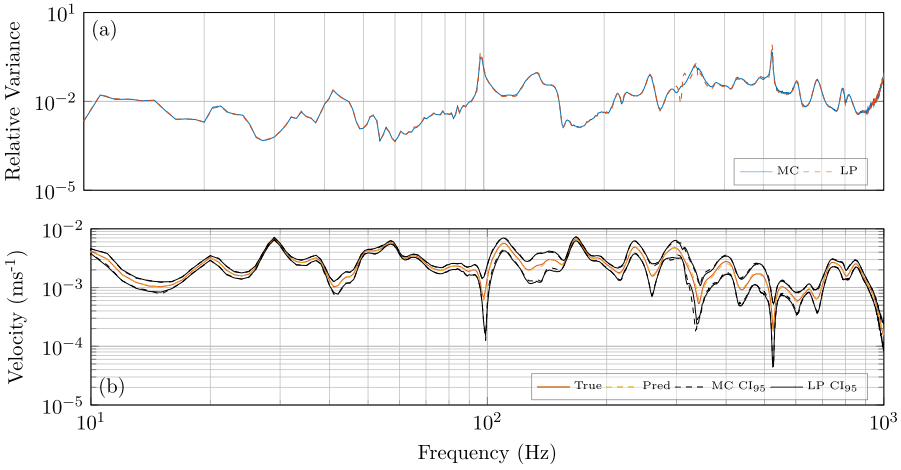

Fig. 9. (a) - Relative variance of the receiver response magnitude, RelVar $\left[|v_{Cb}|\right]$, predicted using the LP framework with Eq. (50) (orange), and a MC propagation (blue). (b) - True (orange) and predicted (yellow) receiver response magnitude $|v_{Cb}|$ with a ±95% confidence bound based on the LP bivariate uncertainty $\mathbf{\Sigma_v}$ and the CI estimation procedure described in section 4.3.1 (solid). Also shown is the ±95% confidence bound based on the MC propagation (dashed). (For interpretation of the references to colour in this figure legend, the reader is referred to the Web version of this article.)

only FRFs that share an excitation are correlated. This non-zero structure is illustrated in Fig. 11a, where the y/x axis labels correspond to matrix row/column indices, respectively. This was necessary as only ten excitations were considered for each FRF, meaning that the uncorrelated covariance terms had not yet reached sufficiently small values. The MC propagation, however, was performed using 2000 realisations, thus providing sufficient observations for the uncorrelated terms to diminish.

Figs. 7 and 8 demonstrate the inverse propagation of uncertainty using the proposed framework. A blocked force TPA also requires the forward prediction of an operational response. Shown in Fig. 9 are the results of the forward propagation in the case that $\mathbf{H_{Cbc}} = \mathbf{H_{Ccb}^T}$ is measured reciprocally (i.e. independently of $\mathbf{Y_{Ccc}}$). In this case the additional covariance term in Eq. (49) is

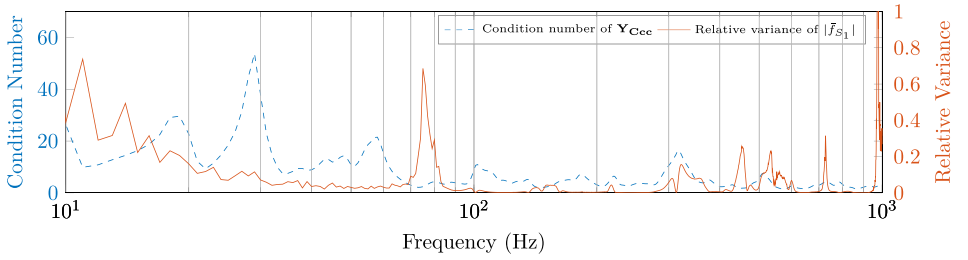

Fig. 10. Condition number of the FRF matrix $\mathbf{Y}_{\mathbf{Cc}}$ compared against the relative variance of the blocked force magnitude $|\bar{f}_{S_1}|$.

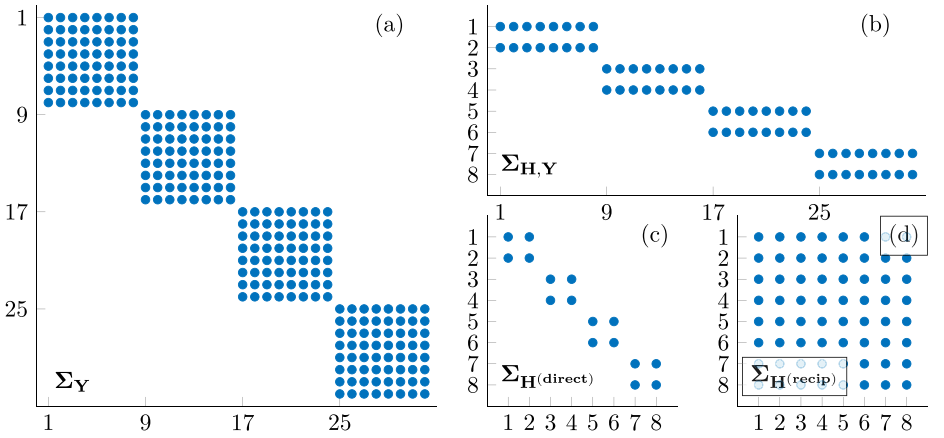

Fig. 11. Non-zero structure of the bivariate FRF covariance matrices: (a) - inverse FRF $\mathbf{Y}_{\mathbf{Ccc}}$, (b) - covariance between inverse and forward FRFs, (c) - forward FRF (direct) $\mathbf{H}_{\mathbf{Cbc}}$, (d) - forward FRF (reciprocal) $\mathbf{H}_{\mathbf{Ccb}}$.

not required, as the inverse and forward FRF matrices are uncorrelated.

Shown in Fig. 9a is the relative variance of the receiver response magnitude $|v_{Cb}|$ (orange), calculated as per Eq. (50), using the proposed framework to estimate the required bivariate response uncertainty $\mathbf{\Sigma}_{\mathbf{v}}$. Also shown (blue) is the result of a MC propagation. Based on Eq. (49), the framework estimation has taken into account the blocked force uncertainty $\mathbf{\Sigma}_{\bar{\mathbf{f}}}$ and the forward FRF uncertainty $\mathbf{\Sigma}_{\mathbf{H}}$ (neglecting the forward/inverse FRF covariance $\mathbf{\Sigma}_{\mathbf{H,Y}}$). Note that as the forward FRF was measured reciprocally (i.e. using a single shared excitation at b), there exist inter-FRF correlations between all of its elements. As such $\mathbf{\Sigma}_{\mathbf{H}}$ is fully populated, as illustrated in Fig. 11d. The MC result was obtained by performing 2000 inverse blocked force and forward response calculations, whilst randomly sampling from the set of inverse FRF, operational velocity, and forward FRF measurements. The absolute value of each response prediction was then taken and the relative variance computed.

The MC and framework estimated uncertainties are in good agreement across the entire frequency range considered. This result confirms a successful propagation of uncertainty. However, it is often more convenient to present an uncertainty relative to its expected value in the form a confidence interval (CI). Shown in Fig. 9b are the true (orange) and predicted (yellow) operational responses. Also shown are two ±95% confidence intervals, obtained using the estimation procedure presented in section 4.3.1, based on the proposed framework (solid) and the MC propagated (dashed) uncertainty. Not only does the LP CI_{95} bound appear to encapsulate the true and predicted response, it is in good agreement with the MC CI_{95} bound across the majority of the frequency range.

It is worth noting that any disagreement may stem from either: the inverse propagation of uncertainty (where a linear assumption is made), the MC propagation (where only 2000 realisations were considered), or the CI estimation (which also relies on a MC sampling).[3] Nevertheless, for the level of input uncertainty considered the framework provides an acceptable level of accuracy.

It is interesting to compare the results of the uncertainty framework with the condition number of the FRF matrix $\mathbf{Y}_{\mathbf{Ccc}}$, as shown in Fig. 10 (blue). Also shown in Fig. 10 is the relative variance of the blocked force magnitude (orange). From this comparison it is clear that the condition number provides a poor indication of which regions are most sensitive to the uncertainty present. For example, around 75 Hz the blocked force magnitude $|\bar{f}_{S_1}|$ has a maximum relative variance. The condition number, however, does not indicate that we should expect large uncertainty here. Similarly, around 30 Hz the condition number suggests

[3] Note that the MC CL_{95} bound was obtained directly from the 2000 realisations performed in the MC propagation. The LP CL_{95} bound was obtained by generating 10000 random samples from the operational response's expected value and bivariate covariance matrix.

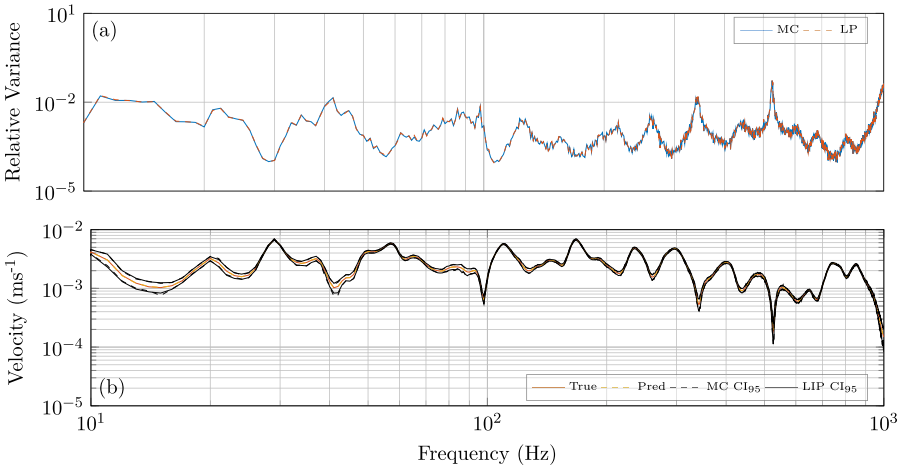

Fig. 12. (a) - Relative variance of the receiver response magnitude, RelVar $\left[|v_{Cb}|\right]$, predicted using the LP framework with Eq. (50) (orange), and a MC propagation (blue). (b) - True (orange) and predicted (yellow) receiver response magnitude $|v_{Cb}|$ with a $\pm$95% confidence bound based on the LP bivariate uncertainty $\boldsymbol{\Sigma}_{\mathbf{v}}$ and the CI estimation procedure described in section 4.3.1 (solid). Also shown is the $\pm$95% confidence bound based on the MC propagation (dashed). (For interpretation of the references to colour in this figure legend, the reader is referred to the Web version of this article.)

that we should expect large uncertainty, where in fact the relative variance is relatively low. These results are in agreement with the discussion of section 6, and justify the use of a more rigorous uncertainty estimate.

Shown in Fig. 12 are the forward propagation results in the case that $\mathbf{H}_{\mathbf{Cbc}}$ is measured directly (i.e. simultaneously to $\mathbf{Y}_{\mathbf{Ccc}}$). In this case the inverse and forward FRF matrices are correlated through their shared excitation, thus we require the additional covariance terms in Eq. (49). When measured directly, excitations are performed at each interface DoF. As we are considering only a single response position b, the forward FRF matrix, $\mathbf{H}_{\mathbf{Cbc}}$, does not possess any inter-FRF correlation. Consequently the covariance matrix $\boldsymbol{\Sigma}_{\mathbf{H}}$ is block diagonal, as illustrated in Fig. 11c.

Notice that there has been a considerable decrease in the relative variance and the associated CI bounds. It happens that when measured directly, the effect of operator uncertainty in the inverse and forward FRF matrices cancel exactly, leaving behind only the velocity's contribution to the uncertainty.

This result may be justified as so. Taking the ith excitation at each interface DoF c, the matrices $\mathbf{Y}_{\mathbf{Ccc_i}}$ and $\mathbf{H}_{\mathbf{Cbc_i}}$ are 'measured'. From $\mathbf{Y}_{\mathbf{Ccc_i}}$ the blocked force $\bar{\mathbf{f}}_{\mathbf{Sc_i}}$ is determined. Note that the excitation position of $\mathbf{Y}_{\mathbf{Ccc_i}}$ defines the position of the blocked force, i.e. by exciting away from the interface the blocked force is defined internally to the source (albeit only slightly). Using the blocked force $\bar{\mathbf{f}}_{\mathbf{Sc_i}}$ and the forward FRF $\mathbf{H}_{\mathbf{Cbc_i}}$ the response at b is predicted. Since the forward FRF is measured from the same position as the 'internal' blocked force, c_i, it correctly predicts the operational response. Since this will be true for all 'realisations', the uncertainty in excitation position does not influence the uncertainty in a response prediction. However, this is only true when: a) excitations are performed solely at the interface, b) operator uncertainty is the primary source of uncertainty, and c) the number of DoFs contributing to the response is matched by the number of DoFs used to define the interface. In the case that measurement uncertainty is present this perfect cancellation would not occur, as the inverse and forward FRFs would be effected by uncorrelated uncertainty. Furthermore, if the blocked force is determined using reciprocal measurements, or over-determined using additional responses positions, perfect cancellation will not occur.

In summary, Figs. 7–12 confirm the validity of the proposed uncertainty propagation framework in the context of a blocked force TPA. In the following section a component-based TPA will be considered, where the forward FRF matrix $\mathbf{H}_{\mathbf{Cbc}}$ is obtained through a dynamic sub-structuring procedure.

8.2. Component-based TPA

In a component-based TPA the forward FRF $\mathbf{H}_{\mathbf{Cbc}}$ is determined by means of dynamic sub-structuring, where the FRFs of each constituent sub-structure are measured independently and coupled together as per section 3. In this example, the source sub-structure used in the above blocked force TPA is coupled to a second receiver, details of which are given in Table 1, and its operational response predicted. The effect of operator uncertainty on the measured source and receiver FRFs, $\mathbf{Y}_{\mathbf{S}} \in \mathbb{C}^{4\times4}$ and $\mathbf{Y}_{\mathbf{R}} \in \mathbb{C}^{5\times5}$, is considered with a value of $\sigma = 0.0026$ in both, twice that used in the blocked force TPA. Based on the measured source and receiver FRFs, the uncoupled (i.e. block diagonal) FRF matrix $[\mathbf{Y}] \in \mathbb{C}^{9\times9}$ is built, and the bivariate covariance matrix $\boldsymbol{\Sigma}_{[\mathbf{Y}]} \in \mathbb{R}^{162\times162}$ is estimated. Note that measurement uncertainty is not considered in the FRFs.

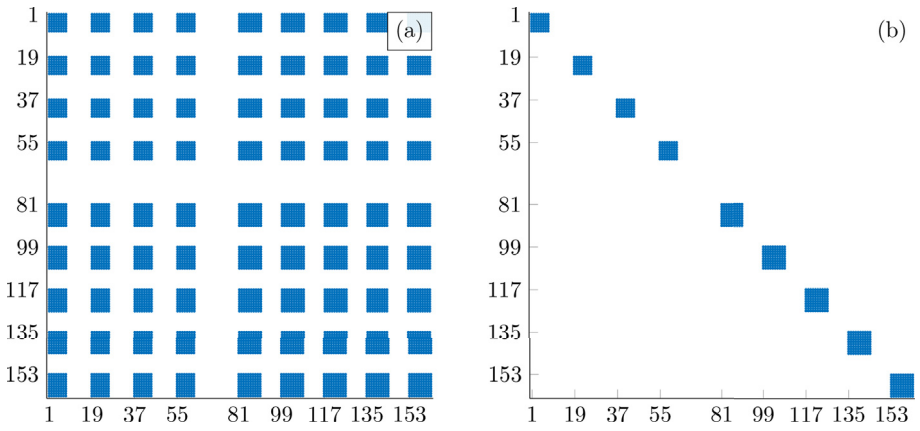

Fig. 13. Non-zero structure of the uncoupled FRF covariance matrix $\mathbf{\Sigma}_{[\mathbf{Y}]}$ under the assumptions of full sub-structure correlation (a), and operator uncertainty only (b).

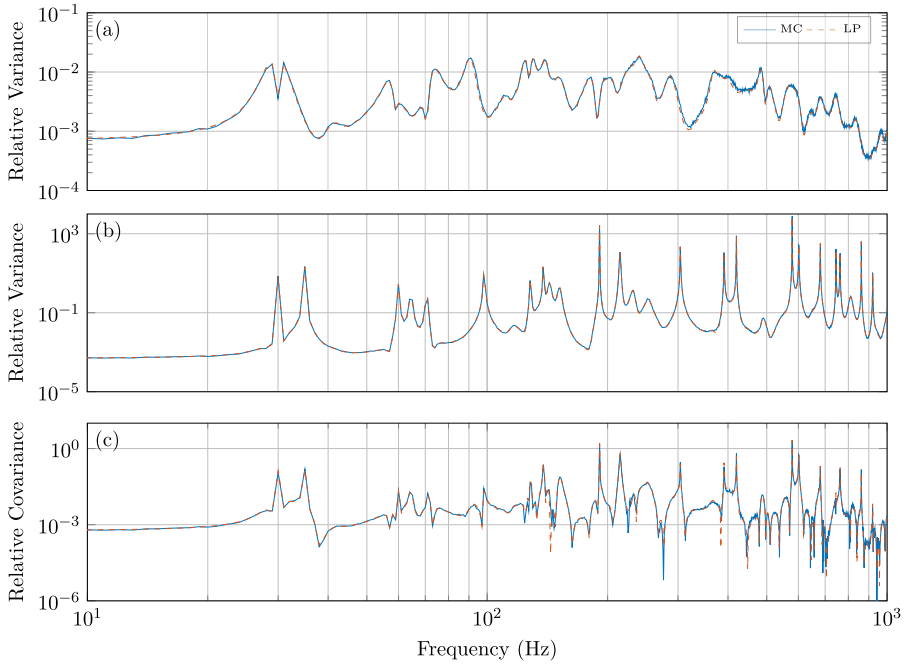

Fig. 14. Bivariate uncertainty in the coupled FRF $H_{C_{51}}$, due to the uncoupled FRF uncertainty $\mathbf{\Sigma}_{[\mathbf{Y}]}$, predicted using the LP framework (orange) and a MC propagation (blue). Operator uncertainty was set at $\sigma = 0.0026$. (a) - RelVar $\left[\text{Re}\left(H_{C_{51}}\right)\right]$, (b) - RelVar $\left[\text{Im}\left(H_{C_{51}}\right)\right]$, (c) - RelCov $\left[\text{Re}\left(H_{C_{51}}\right), \text{Im}\left(H_{C_{51}}\right)\right]$. (For interpretation of the references to colour in this figure legend, the reader is referred to the Web version of this article.)

Although large, relative to the size of the system considered, $\mathbf{\Sigma}_{[\mathbf{Y}]}$ is sparse in structure; the FRF matrices $\mathbf{Y_S}$ and $\mathbf{Y_R}$ are uncorrelated. The non-zero structure of $\mathbf{\Sigma}_{[\mathbf{Y}]}$ is shown in Fig. 13a. Under the assumption of operator uncertainty the columns of each FRF matrix are also uncorrelated with one another. In this case the non-zero structure of $\mathbf{\Sigma}_{[\mathbf{Y}]}$ is shown in Fig. 13b. As only ten excitations are performed for each FRF this non-zero structure was imposed to remove any covariance terms that had not yet diminished sufficiently.

Shown in Fig. 14 are the bivariate uncertainties of the coupled FRF element $H_{C_{51}}$ (i.e. from the interface DoF c_1 to the remote receiver DoF b), due to the operator uncertainty in $\mathbf{Y_S}$ and $\mathbf{Y_R}$. From top to bottom each plot corresponds to: RelVar $\left[\text{Re}\left(H_{C_{51}}\right)\right]$, RelVar $\left[\text{Im}\left(H_{C_{51}}\right)\right]$ and RelCov $\left[\text{Re}\left(H_{C_{51}}\right), \text{Im}\left(H_{C_{51}}\right)\right]$. In blue are the results obtained through a MC propagation, where 2000 FRF matrix realisations are coupled using the dual DS procedure. In orange are the results of the proposed framework (i.e equation (45)). Good agreement is achieved across the entire frequency range of interest.

Shown in Fig. 15a is the relative variance of the coupled FRF magnitude $|H_{C_{51}}|$ (orange) obtained using the proposed framework alongside Eq. (50). Also shown (blue) are the equivalent MC predictions. As expected based on Fig. 14 good agreement is

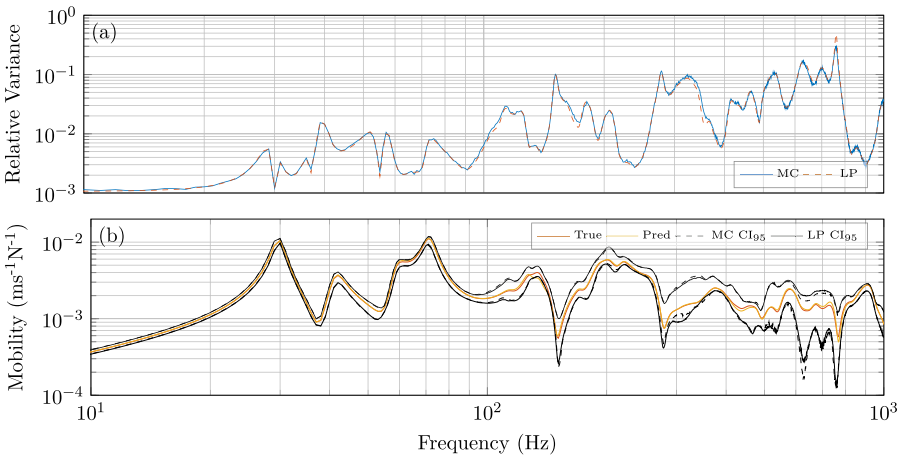

Fig. 15. (a) - Relative variance of the coupled FRF magnitude, RelVar $\left[|H_{C_{51}}|\right]$, predicted using the LP framework with Eq. (50) (orange), and a MC propagation (blue). (b) - True (orange) and predicted (yellow) coupled FRF magnitude $|H_{C_{51}}|$ with a ±95% confidence bound based on the LP bivariate uncertainty $\mathbf{\Sigma_H}$ and the CI estimation procedure described in section 4.3.1 (solid). Also shown is the ±95% confidence bound based on the MC propagation (dashed). (For interpretation of the references to colour in this figure legend, the reader is referred to the Web version of this article.)

obtained. This same result is presented as a ±95% CI in Fig. 15b alongside the true (orange) and predicted (yellow) FRF magnitudes. The CI bounds were estimated using the procedure outlined in section 4.3.1.[4] The two CI bounds are in good agreement across most of the frequency range considered. Again, it is worth noting that any disagreement between these bounds may stem from either: the linearised propagation of uncertainty, the MC propagation, or the CI estimation. Nevertheless, Figs. 14 and 15 demonstrate an accurate propagation of uncertainty through a DS prediction using the proposed framework.

Having propagated the uncoupled FRF uncertainty through a DS prediction, we now have an estimate for the forward FRF, $\mathbf{H}$, and its uncertainty, $\mathbf{\Sigma_H}$. Alongside the blocked force, and its uncertainty $\mathbf{\Sigma_{\bar{f}}}$ (obtained as part of the blocked force TPA), we are now able to estimate the uncertainty in a component-based TPA prediction, as per Eq. (48).

Shown in Fig. 16a is the relative variance of the response magnitude $|v_{Cb}|$ obtained using the proposed framework, alongside Eq. (50). Also shown are the equivalent MC predictions. The MC result was obtained from 4000 realisations, each generated by randomly sampling from the 2000 coupled FRF matrices (obtained from the DS MC propagation) and the 2000 blocked force estimates (obtained from the blocked force MC propagation). Again, good agreement is obtained between the two predictions. This same result is presented as a ±95% CI in Fig. 16b alongside the true (orange) and predicted (yellow) response magnitudes. Again, good agreement is obtained between the two CI bounds, demonstrating an accurate propagation of uncertainty through a component-based TPA prediction.

Having successfully propagated uncertainty through a component-based TPA, we will briefly consider the rank ordering of contributions, and the uncertainty thereof. Shown in Fig. 17a are the magnitude contributions of each interface DoF over the frequency range 10–100 Hz. Also shown in black is the total response magnitude. Notice that at some frequencies the individual contribution magnitudes exceed the total response; this is due to the neglect of phase interactions between the individual contributions. Nevertheless, over the region considered the contributions $|v_{Cb_{(3)}}|$ and $|v_{Cb_{(4)}}|$ appear the most dominant. Given that both $|v_{Cb_{(3)}}|$ and $|v_{Cb_{(4)}}|$ have an associated uncertainty, we are interested in the probability that one (say $|v_{Cb_{(4)}}|$) is greater than the other, $P\left(|v_{Cb_{(4)}}| \geq |v_{Cb_{(3)}}|\right)$. Applying the procedure outlined in section 5 leads to the frequency dependent probability shown Fig. 17b. This probability provides a measure of confidence in the rank ordering of $|v_{Cb_{(3)}}|$ and $|v_{Cb_{(4)}}|$. For example, in the region of 40 Hz, there is a high probability that $|v_{Cb_{(4)}}| \geq |v_{Cb_{(3)}}|$. Similarly, in the region of 65 Hz, there is a high probability that $|v_{Cb_{(3)}}| \geq |v_{Cb_{(4)}}|$. Although this result may be inferred from the magnitudes alone (i.e. Fig. 17a), doing so does not take into account the uncertainty present in a given contribution.

9. Experimental case study

In this section we will demonstrate the proposed uncertainty propagation framework using an experimental case study. The example will consider the in-situ characterisation of blocked forces on the electric steering system shown in Fig. 18a, and the subsequent prediction of an operational response (i.e. an on-board validation). This example is representative of a standard

[4] Note that the MC CL_{95} bound was obtained directly from the 2000 realisations performed in the MC propagation. The LP CL_{95} bound was obtained by generating 10000 random samples from the coupled FRFs expected value and bivariate covariance matrix.

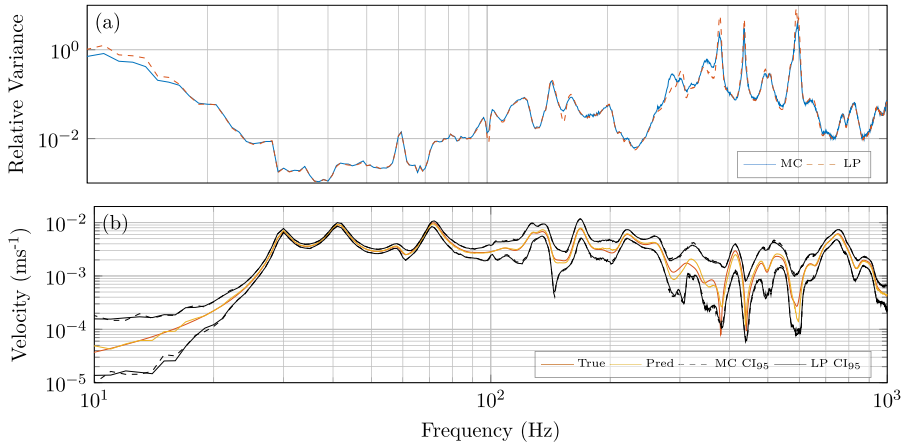

Fig. 16. (a) - Relative variance of the component-based TPA response prediction, RelVar $\left[|v_{Cb}|\right]$, predicted using the LP framework with Eq. (50) (orange), and a MC propagation (blue). (b) - True (orange) and predicted (yellow) response prediction magnitude $|v_{Cb}|$ with a ±95% confidence bound based on the LP bivariate uncertainty $\boldsymbol{\Sigma}_{\mathbf{v}}$ and the CI estimation procedure described in section 4.3.1 (solid). Also shown is the ±95% confidence bound based on the MC propagation (dashed). (For interpretation of the references to colour in this figure legend, the reader is referred to the Web version of this article.)

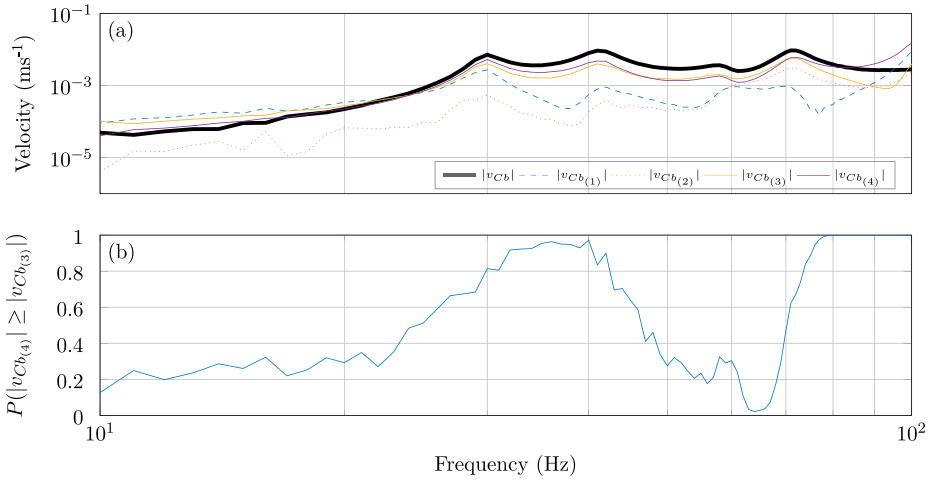

Fig. 17. (a) - Rank ordering of blocked force contributions. (b) - Probability of the contribution magnitude $|v_{Cb_{(4)}}|$ exceeding $|v_{Cb_{(3)}}|$.

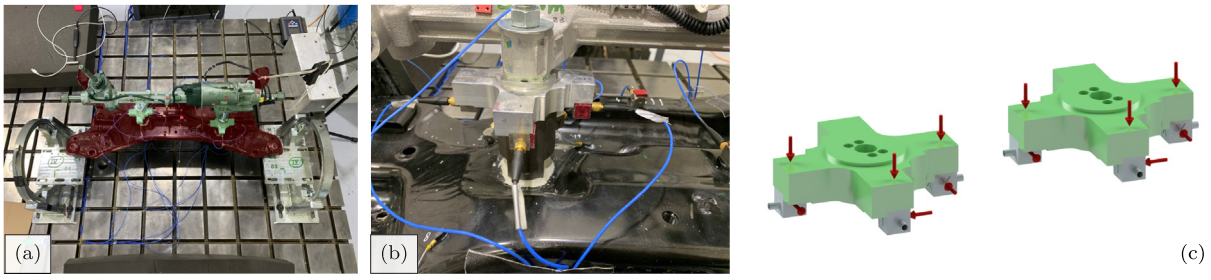

Fig. 18. Experimental case study photos and interface fixtures. An electric steering system coupled to a test bench via two cross-like elements, each instrumented with 3 bi-axial accelerometers. (a) - Steering system coupled to test bench. (b) - Interface coupling close up. (c) - Interface fixtures with applied excitations.

blocked force TPA procedure. Dynamic sub-structuring will not be considered.

The electric steering system is coupled to a representative receiver structure via 2 cross-like elements (see Fig. 18b). These fixtures have been designed to facilitate a characterisation in 6 DoFs (at each foot). Each cross element is instrumented with 3 bi-axial accelerometers as illustrated in Fig. 18c, where red arrows are used to indicate the direction of applied forces in the

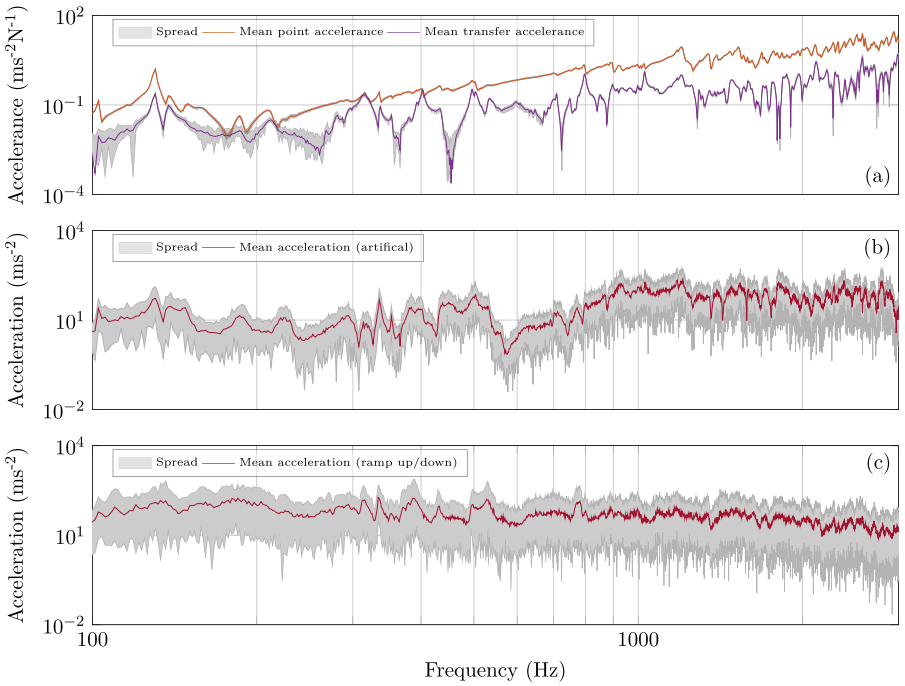

Fig. 19. Examples of uncertainty for the measured accelerance (a) and acceleration: (b) - artificial excitation, (c) - forced ramp up/down.

measurement of assembly FRFs. Also included were a further 6 bi-axial accelerometers on the underside of the receiver structure. These additional DoFs allow for a two-fold over-determination in the blocked force characterisation. A final accelerometer is mounted remote from the interface and is used as a target response for an on-board validation. Note that whilst mobility and velocity notion will be retained, in what follows all results are presented in terms of accelerance and acceleration.

The assembly FRF matrix $\mathbf{Y_C} = \left[\mathbf{Y_{Ccc}}|\mathbf{Y_{Cbc}}\right]^T \in \mathbb{C}^{24\times12}$ (with $\mathbf{Y_{Ccc}} \in \mathbb{C}^{12\times12}$ and $\mathbf{Y_{Cbc}} \in \mathbb{C}^{12\times12}$) was measured using an impact based approach, with 15 repeated excitations at each interface DoF. From these repeated excitations the expected FRF matrices $\mathbf{Y_{Ccc}}$ and $\mathbf{Y_C}$ were calculated, alongside their respective bivariate covariance matrices $\mathbf{\Sigma}_{\mathbf{Y_{Ccc}}} \in \mathbb{R}^{288\times288}$ and $\mathbf{\Sigma}_{\mathbf{Y_C}} \in \mathbb{R}^{576\times576}$. The FRF matrices $\mathbf{Y_{Ccc}}$ and $\mathbf{Y_C}$ are used to calculate, respectively, determined and over-determined blocked forces. Two operational source states are considered. The first is an artificial one, obtained using a shaker driven by constant white noise. The second consists of a repeated forced run up/down manoeuvrer of the steering system. For each case the operational response vectors $\mathbf{v_{Cc}} \in \mathbb{C}^{12}$ and $\mathbf{v_C} = \left[\mathbf{v_{Cc}}|\mathbf{v_{Cb}}\right]^T \in \mathbb{C}^{24}$ are measured. To obtain an appropriate covariance matrix the operational response is recorded for approx. 1 min. This signal is separated into discrete time windows with an overlap of 50%. The phase of each window is then reassigned to an appropriate sensor. These phase corrected time windowed response vectors are then used to estimate the bivariate covariance matrices $\mathbf{\Sigma}_{\mathbf{v_{Cc}}} \in \mathbb{R}^{24\times24}$ and $\mathbf{\Sigma}_{\mathbf{v_C}} \in \mathbb{R}^{48\times48}$.

Shown in Fig. 19 are some examples of the FRF and operational response measurements and their associated uncertainties (for clarity these are shown as max/min bounds). In Fig. 19a a driving point and transfer FRF are shown (max/min bounds are obtained from the 15 repeated excitations). In Fig. 19b an operational response due to an artificial excitation is shown (max/min bounds are obtained across the individual time windows). In Fig. 19c an operational response due to a forced ramp up/down manoeuvrer is shown (max/min bounds are again obtained across the individual time windows).

Note that the operational response uncertainties in Fig. 19b and c are quite broad. This is to be expected, given that we are looking at the total variation of the response over time. If interest lay in the variation of the mean value, the covariance calculated from the total variation may be scaled by the number of windows, as described in section 4.4. This would enable a propagation of uncertainty in the mean value of the response, as opposed to its total variation over time.

Shown in Fig. 20 are the bivariate uncertainties of the blocked force element $\bar{f}_{S_1}$, for the determined case (i.e. using only the interface DoFs), due to the FRF uncertainty $\mathbf{\Sigma}_{\mathbf{Y_{Ccc}}}$ only. Note that for the square FRF matrix $\mathbf{Y_{Ccc}}$ the Jacobian in equation (36) is used to propagate its uncertainty. From top to bottom each plot corresponds to: RelVar $\left[\mathrm{Re}\left(\bar{f}_{S_1}\right)\right]$, RelVar $\left[\mathrm{Im}\left(\bar{f}_{S_1}\right)\right]$, and RelCov $\left[\mathrm{Re}\left(\bar{f}_{S_1}\right), \mathrm{Im}\left(\bar{f}_{S_1}\right)\right]$. The framework predicted uncertainty (orange) is compared against a Monte-Carlo propagation (blue) where 5000 random FRF matrix realisations are inverted and a blocked force calculated for each. The two are in excellent agreement. This indicates a successful propagation of uncertainty through an in-situ blocked force characterisation.

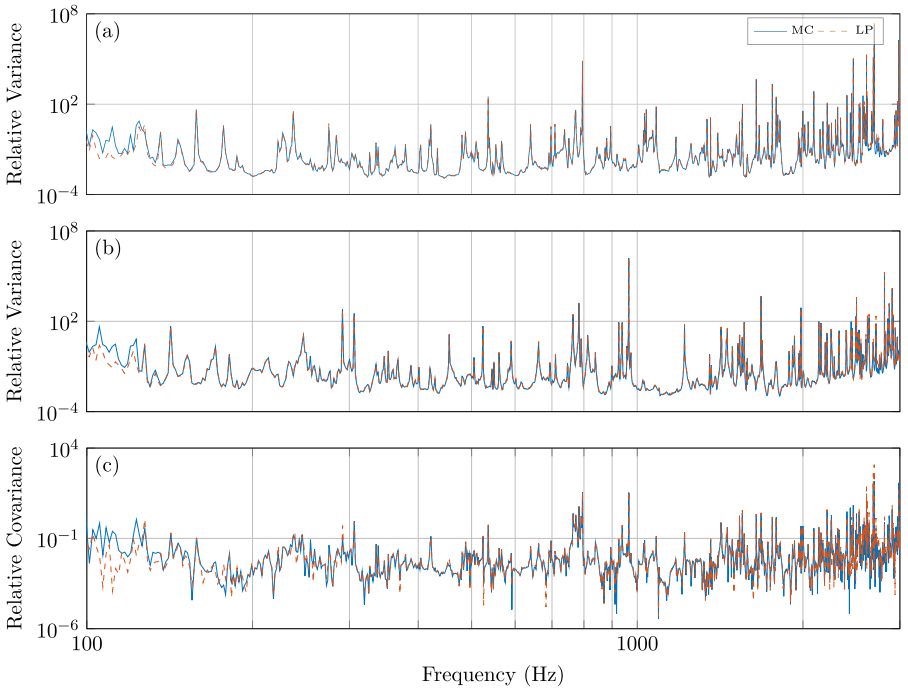

Fig. 20. Bivariate uncertainty in the determined blocked force $\bar{f}_{S_1}$, due to the FRF uncertainty $\boldsymbol{\Sigma}_{\mathbf{Y}_{cc}}$, predicted using the LP framework (orange) and a MC propagation (blue). (a) - RelVar $\left[\mathrm{Re}\left(\bar{f}_{S_1}\right)\right]$, (b) - RelVar $\left[\mathrm{Im}\left(\bar{f}_{S_1}\right)\right]$, (c) - RelCov $\left[\mathrm{Re}\left(\bar{f}_{S_1}\right), \mathrm{Im}\left(\bar{f}_{S_1}\right)\right]$. (For interpretation of the references to colour in this figure legend, the reader is referred to the Web version of this article.)

Shown in Fig. 21 are the bivariate uncertainties of the blocked force element $\bar{f}_{S_1}$, for the over-determined case (i.e. using both interface and remote receiver DoFs), due to the FRF uncertainty $\boldsymbol{\Sigma}_{\mathbf{Y_C}}$ only. Note that for the non-square FRF matrix $\mathbf{Y_C}$ the Jacobian in equation (35) is used to propagate its uncertainty. From top to bottom each plot corresponds to: RelVar $\left[\mathrm{Re}\left(\bar{f}_{S_1}\right)\right]$, RelVar $\left[\mathrm{Im}\left(\bar{f}_{S_1}\right)\right]$, and RelCov $\left[\mathrm{Re}\left(\bar{f}_{S_1}\right), \mathrm{Im}\left(\bar{f}_{S_1}\right)\right]$. The framework predicted uncertainty (orange) is compared against a Monte-Carlo propagation (blue) where 5000 random FRF matrix realisations are pseudo-inverted, and a blocked force calculated for each. The two are in excellent agreement. This indicates a successful propagation of uncertainty through an over-determined blocked force characterisation.

The results of Figs. 20 and 21 are representative of those in the remaining entries of the blocked force bivariate covariance matrix $\boldsymbol{\Sigma}_{\bar{\mathbf{f}}} \in \mathbb{R}^{24\times24}$. In a practical situation, where the blocked force is to be transferred between a component manufacturer and client, the bivariate uncertainty $\boldsymbol{\Sigma}_{\bar{\mathbf{f}}} \in \mathbb{R}^{24\times24}$ should accompany the blocked force $\bar{\mathbf{f}}_{\mathbf{S}}$, thus enabling the client to further propagate the experimental uncertainties present.

It was shown in section 8 that the propagation of response uncertainty is exact, in that its propagating function is linear. For this reason we have chosen to omit the bivariate covariance due to the operational response uncertainty.

Shown in Fig. 22 are the remote response predictions (i.e. on-board validations) for the artificial and forced excitations alongside the upper bound of their associated 95% confidence intervals. The lower bound has been omitted for clarity. In each plot two confidence bounds are presented, one obtained via the proposed framework, and the other via a full MC propagation.

In Fig. 22a the response due to an artificial excitation is shown, with the contribution of source uncertainty being neglected. This result thus demonstrates the successful propagation of FRF uncertainty through both the inverse and forward calculation steps. Note that the inverse and forward FRFs are correlated, and so Eq. (41) is used, as opposed to Eq. (38). In Fig. 22a an additional bound is shown in grey. This corresponds to the propagated uncertainty when neglecting the inverse/forward FRF covariance, i.e. assuming $\boldsymbol{\Sigma}_{\mathbf{H,Y}} = \boldsymbol{\Sigma}_{\mathbf{Y,H}} = \mathbf{0}$. As expected this uncorrelated bound is greater than the true bound (in black), as the inverse/forward FRF correlation has the effect of reducing the level of uncertainty, as was illustrated in the numerical example. This result suggests that, in a practical TPA, measuring indicator and target location FRFs simultaneously may provide a more accurate response prediction.

In Fig. 22b the response due to an artificial excitation is shown including the uncertainty contribution of both the FRFs and source. Note that the covariance $\boldsymbol{\Sigma}_{\mathbf{v}}$ has been left unscaled. As such, the confidence bound represents the limit below which the response magnitude, due to an artificial excitation, would be expected to lie (97.5% of the time). In Fig. 22c the response due to a forced ramp up/down excitation is shown including the uncertainty contribution of both the FRFs and source.

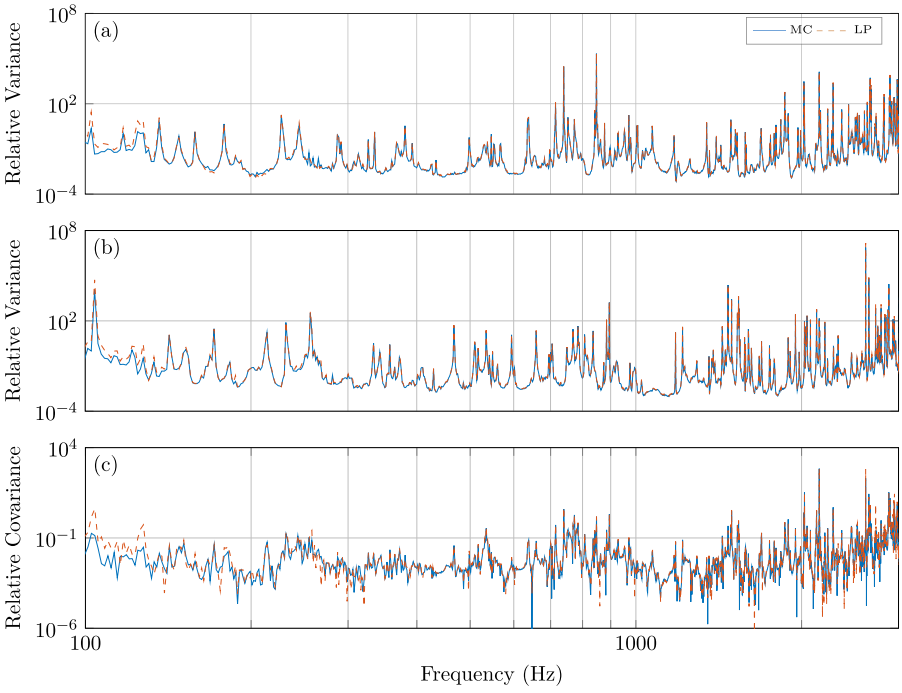

Fig. 21. Bivariate uncertainty in the over-determined blocked force $\bar{f}_{S_1}$, due to the FRF uncertainty $\boldsymbol{\Sigma}_{\mathbf{Y}_c}$, predicted using the LP framework (orange) and a MC propagation (blue). (a) - RelVar $[\mathrm{Re}\,(\bar{f}_{S_1})]$, (b) - RelVar $[\mathrm{Im}\,(\bar{f}_{S_1})]$, (c) - RelCov $[\mathrm{Re}\,(\bar{f}_{S_1})\,,\mathrm{Im}\,(\bar{f}_{S_1})]$. (For interpretation of the references to colour in this figure legend, the reader is referred to the Web version of this article.)

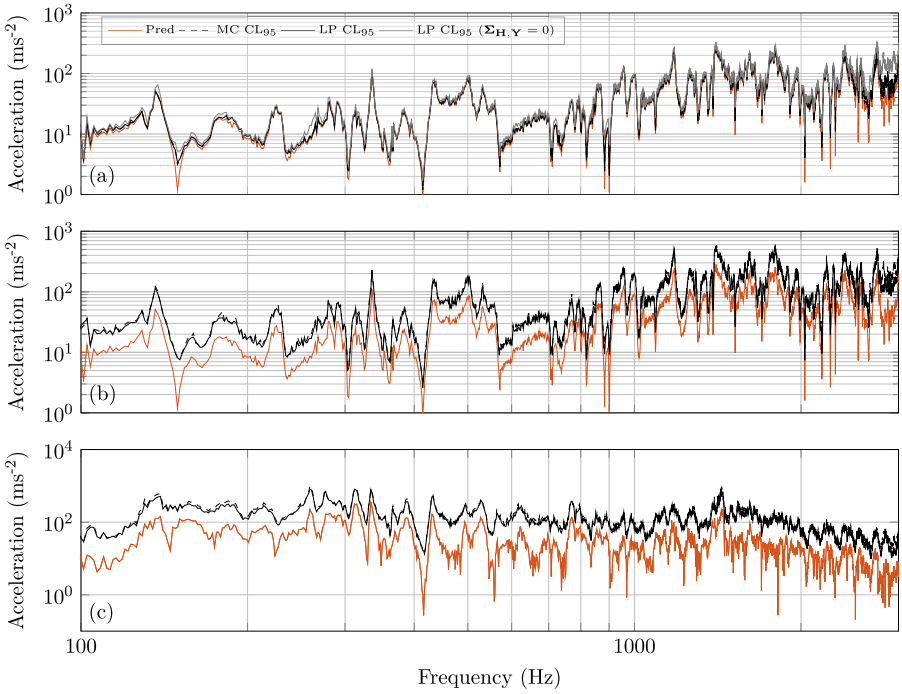

Fig. 22. Operational response prediction for artificial and forced excitations with upper ±95% confidence bounds predicted using the LP framework (solid) and a MC propagation (dashed), with the CI estimation procedure described in section 4.3.1. (a) - Artificial excitation considering only FRF uncertainty. (b) - Artificial excitation considering both FRF and source uncertainty. (c) - Forced ramp up/down excitation considering both FRF and source uncertainty. In (a) an addition upper bound is shown in grey. This corresponds to the case in which the covariance between the inverse and forward FRFs is neglected.

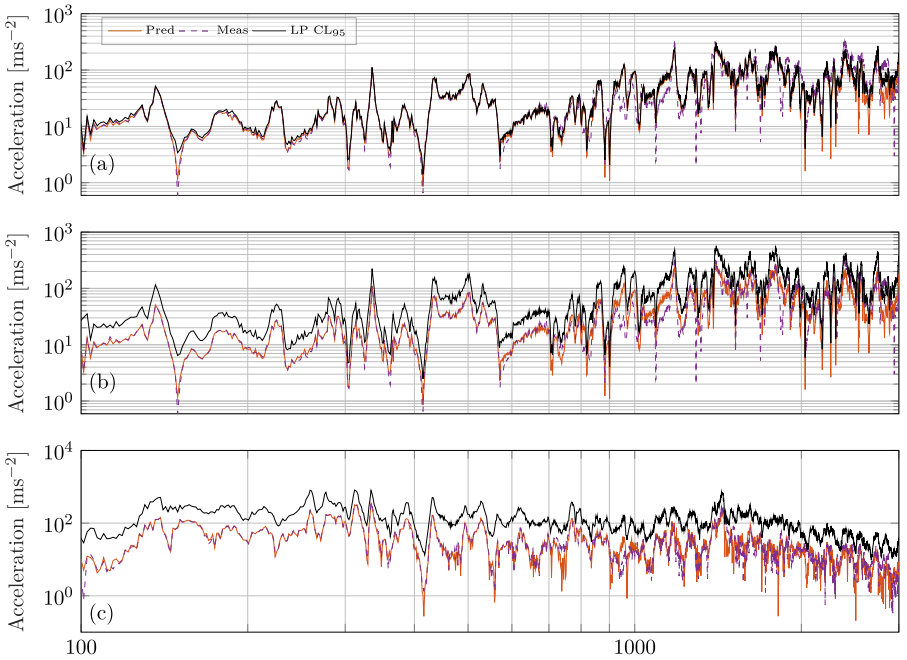

Fig. 23. Measured (purple) and predicted (orange) operational response for artificial and forced excitations with upper ± 95% confidence bounds predicted using the LP framework (black). (a) - Artificial excitation considering only FRF uncertainty. (b) - Artificial excitation considering both FRF and source uncertainty. (c) - Forced ramp up/down excitation considering both FRF and source uncertainty. (For interpretation of the references to colour in this figure legend, the reader is referred to the Web version of this article.)

The results of Fig. 22 demonstrate a successful propagation of both FRF and operational response uncertainty using the proposed framework. The main advantage of the proposed framework, over a standard MC propagation, are two-fold. First, the linear propagation may be performed with far less computation resources. Second, the proposed framework facilitates a more detailed uncertainty analysis, for example the rank ordering of uncertainty contributions, by which is meant the determination of which input uncertainties contribute most to the output uncertainty.

As a final result, Fig. 23 shows the predicted operational response, with its associated confidence bound (as in Fig. 22), alongside the directly measured response. Good agreement is achieved across the entire frequency range, with only minor discrepancies at some frequencies. This suggests that the presence of model uncertainty (i.e. bias errors) was minimal, and so the proposed framework may be applied with confidence.

10. Conclusions

Blocked force and component-based Transfer Path Analysis (TPA) procedures have generated significant interest in recent years, owing to their ease of application, flexibility, and predictive capabilities. This paper addresses the need for a rigorous treatment of their associated uncertainties. Building on the developments of previous works [10,12,13] a combined uncertainty framework is presented for blocked force and component-based TPA procedures. The framework is formulated using a linear covariance propagation and acknowledges both the complex and correlated nature of the underlying uncertainty. Given the symmetry of the underlying equations, the present framework is also applicable to classical (matrix inverse) TPA.

The proposed uncertainty framework comprises three steps. In the first step, Frequency Response Function (FRF) and operational response uncertainty is propagated through an inverse procedure onto the blocked force. If a component-based TPA is considered, step two propagates the sub-structure FRF uncertainty through the chosen Dynamic Sub-structuring (DS) procedure onto the coupled assembly's forward FRF. Finally, in step three, the forward FRF and blocked force uncertainties are propagated onto the TPA response prediction.

The uncertainty framework is summarised through a series of simple equations which can be readily implemented into computer code. Its output is a bivariate covariance matrix that describes the uncertainty in a response prediction (or a blocked force estimation) based on the uncertainty of the experimental data. An advantage of the proposed framework is that it requires no additional experimental effort above what would normally be required.

To accompany the uncertainty propagation, a Monte-Carlo procedure was proposed to determine the magnitude confidence bound of a complex random variable (e.g. a response prediction). Uncertainty in the rank ordering of contributions was also addressed and an appropriate procedure described. Some consideration was given to the condition number, an often-used indicator of uncertainty, and its relation to the proposed framework. Although not the main focus of this paper, the issue of model

uncertainty was also acknowledged and its most likely origins described (i.e. systematic errors due to incompleteness and/or inconsistency).

The framework has been demonstrated both numerically and experimentally, and shown to provide good agreement with Monte-Carlo simulations. Interestingly, it was shown that a considerable reduction in uncertainty can be obtained by measuring indicator and target FRFs simultaneously, as opposed to reciprocally. It was further demonstrated through the numerical example that the condition number of an FRF matrix provides a poor indication of experimental uncertainty compared to the more rigorous framework presented here.

CRediT authorship contribution statement

J.W.R. Meggitt: Conceptualization, Methodology, Validation, Investigation, Writing - original draft, Writing - review & editing. **A.T. Moorhouse:** Writing - review & editing, Supervision, Funding acquisition. **K. Wienen:** Investigation, Validation, Resources. **M. Sturm:** Investigation, Validation, Resources.

Declaration of competing interest

The authors declare that they have no known competing financial interests or personal relationships that could have appeared to influence the work reported in this paper.

Acknowledgements

This work was part funded through the EPSRC Research Grant EP/P005489/1 Design by Science. The authors would like to acknowledge the valuable contributions of A. Clot and R.S Langley from the University of Cambridge.

References

[1] M. van der Seijs, D. de Klerk, D.J. Rixen, General framework for transfer path analysis: history, theory and classification of techniques, Mech. Syst. Signal Process. 68 (2016) 217–244.
[2] A.T. Moorhouse, A.S. Elliott, T.A. Evans, In situ measurement of the blocked force of structure-borne sound sources, J. Sound Vib. 325 (45) (2009) 679–685.
[3] A.S. Elliott, A.T. Moorhouse, T. Huntley, S. Tate, In-situ source path contribution analysis of structure borne road noise, J. Sound Vib. 332 (24) (2013) 6276–6295.
[4] International Organization for Standardization, ISO 20270:2019 Acoustics - Characterization of Sources of Structure-Borne Sound and Vibration - Indirect Measurement of Blocked Forces, 2019.
[5] D. de Klerk, D.J. Rixen, S.N. Voormeeren, General framework for dynamic substructuring: history, review and classification of techniques, AIAA J. 46 (5) (2008) 1169–1181.
[6] A.T. Moorhouse, Virtual acoustic prototypes: listening to machines that don't exist, in: Proceedings of ACOUSTICS 2005, Busselton, Australia, 2005.
[7] M. Sturm, T. Alber, A.T. Moorhouse, D. Zabel, Z. Wang, The in-situ blocked force method for characterization of complex automotive structure-borne sound sources and its use for virtual acoustic prototyping, in: Proceedings of ISMA, Leuven, Belgium, 2016.
[8] J.W.R. Meggitt, A.S. Elliott, A.T. Moorhouse, Virtual assemblies and their use in the prediction of vibro-acoustic responses, in: Proceedings of Acoustics 2016, Warickshire, UK, 2016.
[9] A. Clot, J.W.R. Meggitt, R.S. Langley, A.S. Elliott, A.T. Moorhouse, Development of a hybrid FE-SEA-experimental model, J. Sound Vib. 452 (2019) 112–131.
[10] J.W.R. Meggitt, A.S. Elliott, A.T. Moorhouse, A covariance based framework for the propagation of uncertainty through inverse problems with an application to force identification, Mech. Syst. Signal Process. 124 (2019) 275–297.
[11] S.N. Voormeeren, D. de Klerk, D.J. Rixen, Uncertainty quantification in experimental frequency based substructuring, Mech. Syst. Signal Process. 24 (1) (2010) 106–118.
[12] J.W.R. Meggitt, On the treatment of uncertainty in experimentally measured frequency response functions, Metrologia 55 (2018) 806–818.
[13] J.W.R. Meggitt, A.T. Moorhouse, A covariance based framework for the propagation of correlated uncertainty in frequency based dynamic sub-structuring, Mech. Syst. Signal Process. 136 (2020).
[14] M.H. Kalos, P.A. Whitlock, Monte Carlo Methods, 2 edition, Wiley-VCH, 2009.
[15] Y.I. Bobrovnitskii, A theorem on the representation of the field of forced vibrations of a composite elastic system, Acoust Phys. 47 (5) (2001) 586–589.
[16] A.S. Elliott, J.W.R. Meggitt, A.T. Moorhouse, Blocked forces for the characterisation of structure borne noise, in: Proceedings of Internoise 2015, San Fransisco, USA, 2015.
[17] A.T. Moorhouse, J.W.R. Meggitt, A.S. Elliott, Evaluation of uncertainties in classical and component (blocked force) transfer path analysis (TPA), in: Proceedings of SAE Noise and Vibration Conference & Exhibition, Detroit, USA, 2019.
[18] A. Hjorunges, Complex-Valued Matrix Derivatives, first ed., Cambridge University Press, 2011.
[19] A.N. Thite, D.J. Thompson, The quantification of structure-borne transmission paths by inverse methods. Part 2: use of regularization techniques, J. Sound Vib. 264 (2) (2003) 433–451.
[20] P. Dharmawansa, N. Rajatheva, C. Tellambura, Envelope and phase distribution of two correlated Gaussian variables, IEEE Trans. Commun. 57 (4) (2009) 915–921.
[21] T. Schultz, M. Sheplak, L.N. Cattafesta, Application of multivariate uncertainty analysis to frequency response function estimates, J. Sound Vib. 305 (12) (2007) 116–133.
[22] J.S. Bendat, A.G. Piersol, Random Data: Analysis and Measurement Procedures, fourth ed., John Wiley & Sons, New York, 2010.
[23] J.S. Bendat, Statistical errors in measurement of coherence functions and input/output quantities, J. Sound Vib. 59 (3) (1978) 405–421.
[24] J.S. Bendat, A.G. Piersol, Engineering Applications of Correlation and Spectral Analysis, second ed., John Wiley & Sons, New York, 1993.
[25] G. Strang, Introduction to Linear Algebra, fourth ed., Cambridge Press, 2009.
[26] J.W.R. Meggitt, A.S. Elliott, A.T. Moorhouse, A. Clot, R.S. Langley, Development of a hybrid FE-SEA-experimental model: experimental subsystem characterisation, in: Proceedings of NOVEM: Noise and Vibration - Emerging Methods, Ibiza, Spain, 2018.
[27] J.W.R. Meggitt, A.T. Moorhouse, On the completeness of an interface description and the consistency of blocked forces obtained in-situ, Mech. Syst. Signal Process. 145 (106850) (2020) Elsevier.
[28] J.W.R. Meggitt, A.T. Moorhouse, A.S. Elliott, On the problem of describing the coupling interface between sub-structures: an experimental test for completeness', in: Proceedings of IMAC XVIII, Orlando, USA, 2018.

[29] A.S. Elliott, A.T. Moorhouse, J.W.R. Meggitt, Identification of coupled degrees of freedom at the interface between sub-structures, in: Proceedings of NOVEM: Noise and Vibration - Emerging Methods, Ibiza, Spain, 2018.
[30] K. Wienen, M. Sturm, A.T. Moorhouse, J.W.R. Meggitt, Robust NVH engineering using experimental methods source characterization techniques for component transfer path analysis and virtual acoustic prototyping, in: Proceedings of SAE Noise and Vibration Conference & Exhibition, Detroit, USA, 2019.
[31] L. Meirovitch, Elements of Vibration Analysis, second ed., McGraw-Hill, 1986.